Analysis and development of finite volume methods for the new generation of cubed sphere dynamical cores for the atmosphere

Luan da Fonseca Santos

Report presented to the
Institute of Mathematics and Statistics
of the University of São Paulo
for the Doctor of Science
qualifying examination

Program: Applied Mathematics
Advisor: Prof. Pedro da Silva Peixoto

During the development of this work the author was supported by CAPES and FAPESP (grant number 20/10280-4)

São Paulo
November, 2022

Analysis and development of finite volume methods for the new generation of cubed sphere dynamical cores for the atmosphere

Luan da Fonseca Santos

This is the original version of the
qualifying text prepared by candidate
Luan da Fonseca Santos, as submitted
to the Examining Committee.

Resumo

Luan da Fonseca Santos. **Análise e desenvolvimento de métodos de volumes finitos para modelos da nova geração da dinâmica atmosférica baseados na esfera cubada**. Exame de Qualificação (Doutorado). Instituto de Matemática e Estatística, Universidade de São Paulo, São Paulo, 2022.

O modelo atmosférico global FV3 do GFDL-NOAA-USA, inicialmente desenvolvido para malhas do tipo latitude-longitude, foi adaptado para a esfera cubada visando atingir melhor escalabilidade em super-computadores massivamente paralelos. Entretanto, neste tipo de malhas estamos mais sujeitos à problemas como o grid imprinting. Além disso, o modelo carece de algumas propriedades miméticas, que são altamente desejáveis. Este projeto de doutorado propõe-se a analisar as propriedades das discretizações de volumes finitos utilizadas no modelo FV3 na esfera cubada. Iremos investigar como propriedades das células da esfera cubada interferem na precisão dos esquemas numéricos. O estudo irá começar com a implementação de um código para gerar a esfera cubada e calcular os operados discretos do FV3. Então, iremos analisar como a malha interfere nos modelos de advecção e de águas rasas na esfera.

Palavras-chave: Núcleo dinâmico da atmosfera, esfera cubada, volumes finitos.

Abstract

Luan da Fonseca Santos. **Analysis and development of finite volume methods for the new generation of cubed sphere dynamical cores for the atmosphere**. Qualifying Exam (Doctorate). Institute of Mathematics and Statistics, University of São Paulo, São Paulo, 2022.

The global atmospheric model FV3 from GFDL-NOAA-USA, which was originally designed for latitude-longitude grids, was adapted to the cubed sphere aiming to improve its scalability in massively parallel supercomputers. However, in this kind of grid, we are more likely to have grid imprinting problems. Besides that, the FV3 model lacks some highly desirable mimetic properties. This work aims to analyze the properties of the finite volume discretizations employed in the global atmospheric model FV3 on the cubed-sphere. We will investigate how the properties of the cells may impact on the accuracy of the numerical schemes. This study will firstly implement a cubed-sphere grid generator and the FV3 discrete operators on this grid. Then, we will and analyze how the cubed-sphere grid properties influence in the numerical schemes by assessing it using the advection and shallow-water equations on the sphere. We will study the numerical dispersion and conservations properties of the scheme aiming to propose modifications in the numerical schemes to develop a mimetic finite volume version of the model.

Keywords: Dynamical core, cubed-sphere, finite-volume.

Contents

Appendixes

Chapter 1

Introduction

1.1 Background

Weather and climate predictions are recognized as a good for mankind, due to the information they yield for diverse activities. For instance, short-range forecasts are useful for public use, while medium-range forecasts are helpful for industrial activities and agriculture. Seasonal forecasts (one up to three months) are important to energy planning and agriculture. At last, longer-range forecasts (one century, for instance) are useful for climate change projections that are important for government planning.

The first global Numerical Weather Prediction models emerged in the 1960s with applications to weather, seasonal and climate forecasts. All these applications are essentially based on the same set of Partial Differential Equations (PDEs) but with distinct time scales (Williamson, 2007). These PDEs are defined on the sphere and model the evolution of the atmospheric fluid given the initial conditions. One important component of global models is the dynamical core, which is responsible for solving the PDEs that governs the atmosphere dynamics on grid-scale. The development of numerical methods for dynamical cores has been an active research area since the 1960s.

Global models use the sphere as the computational domain and therefore they require a discretization of the sphere. The first global models used the latitude-longitude grid (Figure 1.1a), which is very suitable for finite-differences schemes due to its orthogonality. The major drawback of the latitude-longitude grid is the clustering of points at the poles, known as the "pole problem", which leads to extremely small time steps for explicit-in-time schemes due to the Courant-Friedrichs-Lewy (CFL) condition, making these schemes computationally very expensive.

The most successful method adopted in global atmospheric dynamical cores that overcomes the CFL restriction is the Semi-Implicit Semi-Lagrangian (SI-SL) scheme (Randall et al., 2018), which emerged in the 1980s and consists of the Lagrangian advection scheme applied at each time-step and the solution of fast gravity waves implicitly, allowing very large time steps despite the pole problem. The SI-SL approach combined with finite differences is still used nowadays, for instance in the UK Met Office global model ENDGame (Benacchio & Wood, 2016; Wood et al., 2014). The expensive part of the SI-SL approach is to

solve an elliptic equation at each time step, that comes from the semi-implicit discretization, which requires global data communication, being inefficient to run in massive parallel supercomputers. Besides that, Semi-Lagrangian schemes are inherently non-conservatives for mass, which is critical for climate forecasts (Williamson, 2007).

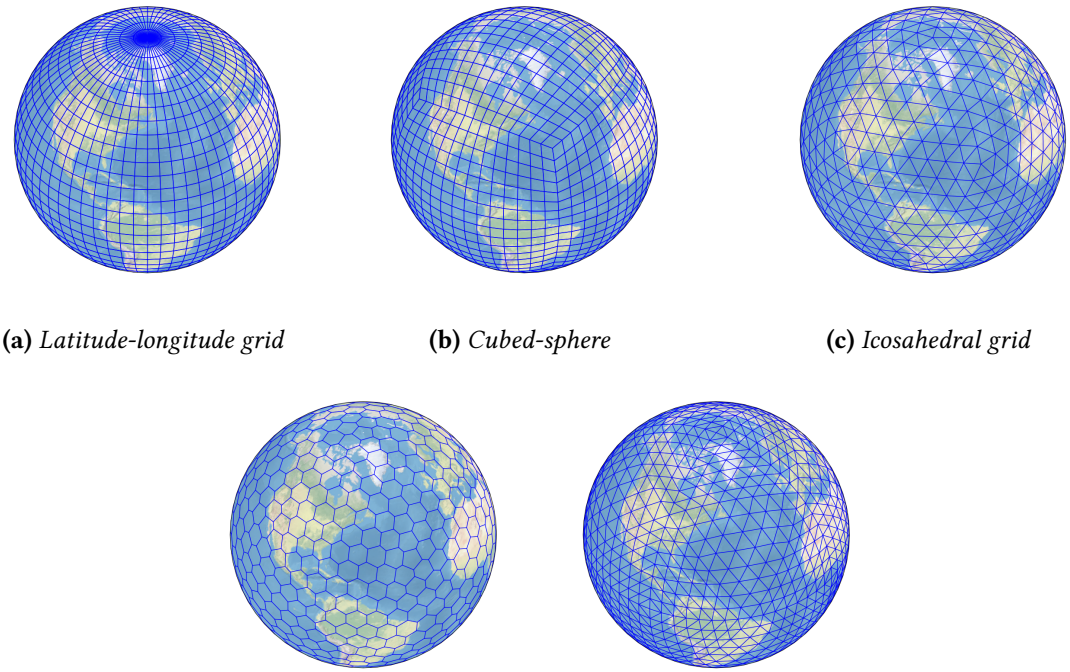

(a) *Latitude-longitude grid* **(b)** *Cubed-sphere* **(c)** *Icosahedral grid*

(d) *Pentagonal/Hexagonal grid* **(e)** *Octahedral grid*

Figure 1.1: *Examples of spherical grids: latitude-longitude grid (a) and grids based on Platonic solids (b)-(d).*

The emergence of the Fast Fourier Transform (FFT) in the 1960s with the work from Cooley and Tukey (1965) allowed the computation of discrete Fourier transforms with $N \log(N)$ complexity. The viability of the usage of FFTs for solving atmospheric flows was shown by Orszag (1970), using the barotropic vorticity equation on the sphere, and by Eliasen et al. (1970), using the primitive equations. The spectral transform method expresses latitude-longitude grid values, that represent some scalar field, using truncated spherical harmonics expansions, which consists of Fourier expansions in latitude circles and Legendre functions expansions in longitude circles. The coefficients in the spectral expansions are known as spectral coefficients and are usually thought to live in the so-called spectral space. Given the grid values, the spectral coefficients are obtained by performing a FFT followed by a Legendre Transform (LT). Conversely, given the spectral coefficients, the grid values are obtained by performing an inverse LT followed by an inverse FFT. The main idea of the spectral method is to apply the spectral transform, in order to go the spectral space, and evaluate spatial derivatives in the spectral space, which consists of multiplying the spectral coefficients by constants. Then, the method performs the inverse spectral transform in order to get back to grid space, and the nonlinear terms are treated on the grid space (Krishnamurti et al., 2006).

The spectral transform makes the use of SI-SL methods computationally cheap, since the solution to elliptic problems becomes easy, once the spherical harmonics are eigenfunctions of the Laplacian operator on the sphere. Therefore, the spectral transform method gets faster when combined with the SI-SL approach due to the larger times-steps allowed in this case. Due to these enhancements, the spectral transform dominated global atmospheric modeling (Randall et al., 2018) since the 1980s. Indeed, the spectral method is still used in many current operational Weather Forecasting models such as the Integrated Forecast System (IFS) from European Centre for Medium-Range Weather Forecasts (ECMWF), Global Forecast System (GFS) from National Centers for Environmental Prediction (NCEP) and the Brazilian Global Atmospheric Model (BAM) (Figueroa et al., 2016) from Center for Weather Forecasting and Climate Research [Centro de Previsão de Tempo e Estudos Climáticos (CPTEC)].

With the beginning of the multicore era in the 1990s, the global atmospheric models started to move towards parallel efficiency aiming to run at very high resolutions. Even though the spectral transform expansions have a global data dependency, some parallelization is feasible among all the computations of FFTs, LTs and their inverses (Barros et al., 1995). However, the parallelization of the spectral method requires data transpositions in order to compute FFTs and LTs in parallel. These transpositions demand a lot of global communication using, for instance, the Message Passing Interface (MPI) (Zheng & Marguinaud, 2018). Indeed, the spectral transform becomes the most expensive component of global spectral models when the resolution is increased due to the amount of MPI communications (Müller et al., 2019).

The adiabatic and frictionless continuous equations that govern the atmospheric flow have conserved quantities. Among them, some of the most important are mass, total energy, angular momentum and potential vorticity (Thuburn, 2011). Numerical schemes that are known for having discrete analogous of these conservative properties are known as mimetic schemes. As we pointed out, Semi-Lagrangian schemes lack mass conservation. Nevertheless, these schemes have been employed in dynamical cores for better computational performance. However, dynamical cores should have discrete analogous of the continuous conserved quantities, especially concerning for longer simulation runs.

Aiming for better performance in massively parallel computers and conservation properties, new dynamical cores have been developed since the beginning of the 2000s. Novel spherical grids have been proposed, in order to avoid the pole problem. A popular choice are grids based on Platonic solids (Staniforth & Thuburn, 2012). The construction of these grids relies on a Platonic circumscribed on the sphere and the projection of its faces onto the sphere, which leads to quasi-uniform and more isotropic spherical grids. Some examples of spherical grids based on Platonic solids employed in the new generation of dynamical cores are the cubed-sphere (Figure 1.1b), icosahedral grid (Figure 1.1c), the pentagonal/hexagonal or Voronoi grid (Figure 1.1d) and octahedral grid (Figure 1.1e), which are based on the cube, icosahedron, dodecahedron and octahedron, respectively (Ullrich et al., 2017).

1.2 Motivations

The cubed-sphere became a popular quasi-uniform grid for the new generation of dynamical cores. It was originally proposed by Sadourny (1972) and it was reviseted by Ronchi et al. (1996). Some of the cubed-sphere advantages are: uniformity; quadrilateral structure, making the grid indexing trivial; no overlappings; it is cheap to generate. However, the major drawbacks of the cubed-sphere are: non-orthogonal coordinate system, which leads to metric terms on the differetial operator; discontinuity of the coordinate system at the cube edges, which may generate numerical noise and demands special treatment of discrete operators at the cube edges.

Despite of its drawbacks, the cubed-sphere has been adpoted in some of the new generation dynamical cores. For instance, the cubed-sphere is used in the Community Atmosphere Model (CAM-SE) from the NCAR using spectral elements (Dennis et al., 2012) and in the Nonhydrostatic Unified Model of the Atmosphere (NUMA) from the US Navy using Discontinuous Galerkin methods (Giraldo et al., 2013). The cubed-sphere was also chosen to be used in the next UK Met Office global model using mixed finite elements (Kent et al., 2022). At last, the Finite Volume Cubed-Sphere dynamical core (FV3) from the Geophysical Fluid Dynamics Laboratory (GFDL) and the National Oceanic and Atmospheric Administration (NOAA) (Harris & Lin, 2013; Putman & Lin, 2007) is another example of new generation dynamical core based on the cubed-sphere.

The FV3 model is an extension of the Finite-Volume dynamical core (FVcore) from latitude-longitude grids to the cubed-sphere. The numerical methods from FVcore started to be developed with the transport scheme from the work Lin et al. (1994), which is based on the piecewise linear scheme from Van Leer (1977). This scheme was later improved, using the Piecewise Parabolic Method (PPM) (Carpenter et al., 1990; Colella & Woodward, 1984) using dimension splitting techniques that guarantee monotonicity and mass conservation, for the transport equation (Lin & Rood, 1996) and the shallow-water equations (Lin & Rood, 1997). An important feature is that the FVcore combines the Arakawa C- and D-grids (Arakawa & Lamb, 1977), where the C-grid values are computed in and intermediate time step. The full global model was then presented by Lin (2004).

The FVcore was adapted to the cubed-sphere grid (Putman, 2007; Putman & Lin, 2007), to reach better performance in parallel computers, leading to the FV3 model. Later, the FV3 also was improved to allow locally refinement grids through grid-nesting or grid-stretching (Harris & Lin, 2013). Currently, the FV3 model is capable of perfoming hydrostatic and non-hydrostatic atmospheric simulations and it was chosen as the new US global weather prediction model, indeed, it replaced the spectral transform Global Forecast System (GFS) in June, 2019 (Samenow, 2019).

However, a well-known problem that occurs on cubed-sphere models that use low-order numerical methods is the grid imprinting visible due to the coordinate system discontinuity, especially at larger scales, leading to the emergence of a wavenumber 4 pattern. This was reported in the paper of Rančić et al. (2017), where the authors employ a finite-difference numerical scheme on the Uniform Jacobian cubed-sphere using a Arakawa B-grid. The unpublished report from Whitaker (2015) shows grid imprinting in other models, including the FV3. Generally speaking, grid imprinting is the presence of artificial behaviors on

the numerical solution that is associated with the grid employed. It is important to stress out that other quasi-uniform grids may also suffer from grid imprinting. For instance, a popular mimetic method, known as TRiSK, was proposed in the literature by Thuburn et al. (2009) and Ringler et al. (2010) using finite difference and finite volume schemes. This scheme is designed for general orthogonal grids, such as the Voronoi and icosahedral grids, and ensures mass and total energy conservation. This method has been employed in the dynamical core of the Model for Prediction Across Scales (MPAS) from National Center for Atmospheric Research (NCAR) (Skamarock et al., 2012), which intended to work on general Voronoi grids, including locally refined Voronoi grids. However, the TRiSK scheme is a low-order scheme and also suffers from grid imprinting, *i.e.*, geometric properties of the grid, such as cell alignment, interfere with the method accuracy (Peixoto, 2016; Peixoto & Barros, 2013; Weller, 2012). Furthermore, in locally refined Voronoi grids, the scheme may become unstable due to ill-aligned cells and numerical dissipation is needed (Santos & Peixoto, 2021), breaking the total energy conservation of the method.

Despite being chosen as the new US global weather prediction model, there is a lack of numerical studies of the FV3 discretizations in the literature, especially regarding the grid imprinting problem and its mimetic properties. For instance, numerical results for the advection equation on the cubed-sphere using the FV3 dynamical core was presented in Putman and Lin (2007). Many other papers available in the literature use the complete FV3 model in three-dimensional frameworks which make it harder to perform a numerical analysis study due not only to its computational cost, but also due to the complexity of three-dimensional atmospheric models. There are no works published in intermediate two-dimensional frameworks, using, for instance, the shallow-water equations on the sphere. Even though the advection equation on the sphere plays a key role in the dynamical core development, since it models the transport of scalar fields on the sphere, important features captured by the shallow-water equations on the sphere, such as the Coriolis effect, inertia-gravity waves, geostrophic adjustment, Rossby waves, among others, are not captured by a simple advection model. Hence, shallow-water equations provide an excellent benchmark to assess dynamical cores in general, since it is only two-dimensional but is a complex enough geophysical model for atmosphere dynamics.

1.3 Goals

The aim of this work is to fill the gap in the literature regarding numerical studies of the FV3 discrete operators that we pointed out before. More explicitly, the goals of this work are:

- Investigate the occurrence of grid imprinting on the cubed-sphere using the advection equations and the shallow-water equations on the sphere;
- Propose improvements on the FV3 discrete operators and modifications on the cubed-sphere that alleviate grid imprinting;
- Investigate how we can add more mimetic properties to the FV3 discretizations.

1.4 Outline

This report is outlined as follows. Chapter 2 is dedicated to review the Piecewise Parabolic Method (PPM) for the one-dimensional advection equation. Chapter 3 reviews the dimension splitting method, which allow us to use one-dimensional methods, such as the PPM, to solve the two-dimensional advection equation. Chapter 4 introduces the cubed-sphere grid and shows some of its geometric properties. Chapter 5 extends the ideas of Chapter 3 to the cubed-sphere grid. The dimension-splitting method on each cubed-sphere panel works as in the plane, with the addtion of metric terms, due to non-orthogonality of the grid, and interpolation between panels to obtain ghost cells values needed for stencil computations. We give some future work perspectives in Chapter 6.

Chapter 2

One-dimensional finite-volume methods

The main aim of this chapter is to give a detailed desctription of the Piecewise Parabolic Method (PPM). We start with a basic review on one-dimensional conservation laws in the integral form in Section 2.1, and in Section 2.2 we set the framework of general one-dimensional finite-volumes schemes. Section 2.3 presents and analyses the PPM in Subsection 2.3.1. Subsection 2.3.2 is dedicated to PPM monotonization and Subsection 2.3.3 is dedicated to the PPM flux.

2.1 One-dimensional system of conservation laws in integral form

In this section, we are going to present the derivation of one-dimensional system of conservation laws in the integral form. The derivation presented here follows LeVeque (1990) and LeVeque (2002) closely and will be useful to fix some notation. Let us assume that x and t represent the spatial and time coordinate, respectively. Given $[x_1, x_2] \subset \mathbb{R}$, $x_1 \leq x_2$, and a time interval $[t_1, t_2] \subset]0, +\infty[$, $t_1 \leq t_2$, our aim is to describe how m state variable densities given by functions $q_1, \cdots, q_m : \mathbb{R} \times [0, +\infty[\to \mathbb{R}$ evolve within time in the considered time interval, assuming that we have neither sinks nor sources for the mass of each state variable and also assuming that the mass flow rate is known for all the state variables.

To set the problem in more mathematical terms, let us denote by $q : \mathbb{R} \times [0, +\infty[\to \mathbb{R}^m$, $q = q(x, t)$, the vector of state variables, *i.e.*, $q_k = q_k$ for $k = 1, \cdots, m$. The mass of q in $[x_1, x_2]$ at time t is defined by:

$$M_{[x_1,x_2]}(t) := \int_{x_1}^{x_2} q(x, t)\, dx \in \mathbb{R}^m. \tag{2.1}$$

Thus, the mass in $[x_1, x_2]$ of the k-th state variable q_k is equal to $(M_{[x_1,x_2]}(t))_k$, $\forall k = 1, \cdots, m$. We are going to assume the following physical constraints concerning the total

mass of each state variable:

1. No mass is created;
2. No mass is destroyed.

Also, let us assume that the mass flow rate in a point x and at a time $t > 0$ is given by $f(q(x,t))$, where $f : \mathbb{R}^m \to \mathbb{R}^m$ is a continuously differentiable (C^1) function. This function f is known as flux function. With the physical constraints that we imposed, the following equation must hold for the mass:

$$\frac{d}{dt}\left(\int_{x_1}^{x_2} q(x,t)\,dx \right) = f(q(x_1,t)) - f(q(x_2,t)). \tag{2.2}$$

Equation (2.2) is known as a conservation law written in integral form and tell us how the mass $M_{[x_1,x_2]}(t)$ varies with time. Another integral form of the conservation law may be obtained integrating Equation (2.2) with respect to time in $[t_1, t_2]$ leading to:

$$\int_{x_1}^{x_2} q(x,t_2)\,dx = \int_{x_1}^{x_2} q(x,t_1)\,dx + \int_{t_1}^{t_2} f(q(x_1,t))\,dt - \int_{t_1}^{t_2} f(q(x_2,t))\,dt. \tag{2.3}$$

Assuming that q is a C^1 function, we may write:

$$\int_{t_1}^{t_2} \frac{\partial}{\partial t} q(x,t)\,dt = q(x,t_2) - q(x,t_1), \tag{2.4}$$

and

$$\int_{x_1}^{x_2} \frac{\partial}{\partial x} f(q(x,t))\,dx = f(q(x_2,t)) - f(q(x_1,t)). \tag{2.5}$$

Replacing Equations (2.4) and (2.5) in (2.3) we get the differential form of the conservation law:

$$\int_{t_1}^{t_2} \int_{x_1}^{x_2} \left(\frac{\partial}{\partial t} q(x,t) + \frac{\partial}{\partial x} f(q(x,t)) \right) dx\,dt = 0. \tag{2.6}$$

Since Equation (2.6) must hold for all x_1, x_2, t_1 and t_2 such that $[x_1, x_2] \times [t_1, t_2] \subset \mathbb{R}\times]0, +\infty[$, we obtain the differential form of the conservation law:

$$\frac{\partial}{\partial t} q(x,t) + \frac{\partial}{\partial x} f(q(x,t)) = 0, \quad \forall (x,t) \in \mathbb{R}\times]0, +\infty[. \tag{2.7}$$

We shall assume that the eigenvalues of the Jacobian matrix of the flux function $Df(q)$ are all real and that $Df(q)$ is a diagonalizable matrix, $\forall q \in \mathbb{R}^m$, so that Equation (2.7) is a hyperbolic partial differential equation (LeVeque, 1990). As we will specify latter, some initial condition will also be supposed to be known as well.

Many physical relevant equations may be written as Equation (2.7). Some examples are the Euler equations for gas dynamics, obtained when $m = 3$, and the one-dimensional shallow-water equations, obtained $m = 2$. Another relevant equations are the Burgers

equation, which is obtained when $m = 1$ and $f(q) = q^2$. The Burgers equation is well known for developing shocks, even for smooth initial conditions and is a simple prototype to study shock formation. At last, the linear advection equation is another interesting example, which is obtained when $m = 1$ and $f(q(x,t)) = u(x,t)q(x,t)$, where $u(x,t)$ is a given velocity. Strictly speaking, the linear advection is not in the form given by Equation (2.7) since f depends on q but also on (x,t). But, one may check that Equation (2.7) is still hyperbolic in this case. The linear advection equation will play a key role in this work due to its importance to development of atmospheric dynamical cores.

We say that q is a strong or classical solution to the conservation law (2.7) if it is C^1 and satisfies the Equation (2.7). Applying the steps from Equation (2.3) to Equation (2.7) in a reverse order, one may check that if q is a strong solution, then it satisfies the integral form (2.3) for all x_1, x_2, t_1 and t_2 such that $[x_1, x_2] \times [t_1, t_2] \subset \mathbb{R}\times]0, +\infty[$. Therefore, Equations (2.3) and (2.7) are equivalent when q is C^1. However, the problem (2.3) can be formulated to functions that are not C^1 and have discontinuities. More generally speaking, we say that $q \in L^\infty(D, \mathbb{R}^m)$ [1] if it satisfies the Equation (2.3) for all x_1, x_2, t_1 and t_2 such that $[x_1, x_2]\times[t_1, t_2] \subset \mathbb{R}\times]0, +\infty[$. It can be shown that this notion of weak solution is equivalent to requiring that (LeVeque, 1990):

$$\int_{-\infty}^{+\infty}\int_{0}^{+\infty}\left(\frac{\partial}{\partial t}\phi(x,t)q(x,t) + \frac{\partial}{\partial x}\phi(x,t)f(q(x,t))\right)dt\,dx = \int_{-\infty}^{+\infty}\phi(x,0)q(x,0)\,dx, \tag{2.8}$$

$\forall\phi \in C_0^1(\mathbb{R}\times[0,+\infty[)$ where $C_0^1(\mathbb{R}\times[0,+\infty[)$ denotes the set of all continuously differentiable functions with compact support in $\mathbb{R} \times [0, +\infty[$. This formulation of weak solution is more common employed on the construction of Discontinuous Galerkin methods (Nair et al., 2011).

In order to develop finite-volume methods for system of conservation laws, it is useful to define the vector of average values of the state variable vector q in the interval $[x_1, x_2]$ at a time t by:

$$Q(t) = \frac{1}{\Delta x}\int_{x_1}^{x_2} q(x,t)\,dx \in \mathbb{R}^m, \tag{2.9}$$

where $\Delta x = x_2 - x_1$. The Equation (2.2) may be rewritten in terms of Q as:

$$\frac{d}{dt}Q(t) = \frac{1}{\Delta x}(f(q(x_1,t)) - f(q(x_2,t))), \tag{2.10}$$

and so is Equation (2.3):

$$Q(t_2) = Q(t_1) + \frac{1}{\Delta x}\left(\int_{t_1}^{t_2} f(q(x_1,t))\,dt - \int_{t_1}^{t_2} f(q(x_2,t))\,dt\right). \tag{2.11}$$

To move towards finite volume schemes, we will restrict our attention to a conservation law in a bounded domain of the form $D = [a, b] \times [0, T]$, $a < b$, $T > 0$. However, we must impose some boundary condition. One possible way and that we will adopted in text are

[1] $L^\infty(D, \mathbb{R}^m) = \{q : D \to \mathbb{R}^m$ such that q is bounded.$\}$

the periodic boundary conditions:

$$q(a,t) = q(b,t), \quad \forall t \in [0,T]. \tag{2.12}$$

Also, we assume that an initial condition $q_0(x) = q(x,0)$, $q_0 \in L^\infty([a,b],\mathbb{R}^m)$, is given. Thus, we have specified a Cauchy problem. We notice that Equations (2.10) and (2.11) hold for all x_1, x_2, t_1 and t_2 such that $[x_1,x_2]\times[t_1,t_2] \subset D$. So, let us discretize the domain D and write Equations (2.10) and (2.11) in terms of this discretization. Given a positive integer N_T, we define the time step $\Delta t = \frac{T}{N_T}$, $t_n = n\Delta t$, for $n = 0, 1, \cdots, N_T$. For the spatial discretization, we consider an uniformly spaced partition of $[a,b]$ given by:

$$[a,b] = \bigcup_{i=1}^{N} X_i, \text{ where } X_i = [x_{i-\frac{1}{2}}, x_{i+\frac{1}{2}}] \text{ and } a = x_{\frac{1}{2}} < x_{\frac{3}{2}} < \cdots < x_{N-\frac{1}{2}} < x_{N+\frac{1}{2}} = b. \tag{2.13}$$

Each interval X_i is referred to as control volume. We shall use the notations $\Delta x = x_{i+\frac{1}{2}} - x_{i-\frac{1}{2}}$ and $x_i = \frac{1}{2}(x_{i+\frac{1}{2}} + x_{i-\frac{1}{2}})$, $\forall i = 1, \cdots, N$, to define the control volume length and midpoint, respectively. We also denote by $Q_i(t) \in \mathbb{R}^m$ as the vector of average values of state variable vector at time t in the control volume X_i, $\forall i = 1, \cdots, N$. Replacing t_1, t_2, x_1 and x_2 by $t_n, t_{n+1}, x_{i-\frac{1}{2}}$ and $x_{i+\frac{1}{2}}$, respectively, in Equation (2.10), we get:

$$\frac{d}{dt}Q_i(t) = \frac{1}{\Delta x}(f(q(x_{i-\frac{1}{2}},t)) - f(q(x_{i+\frac{1}{2}},t))), \quad \forall i = 1, \cdots, N. \tag{2.14}$$

Similarly, Equation (2.11) becomes:

$$Q_i(t_{n+1}) = Q_i(t_n) + \frac{1}{\Delta x}\left(\int_{t_n}^{t_{n+1}} f(q(x_{i-\frac{1}{2}},t))\,dt - \int_{t_n}^{t_{n+1}} f(q(x_{i+\frac{1}{2}},t))\,dt\right), \quad \forall i = 1, \cdots, N, \quad \forall n = 1, \cdots, N_T. \tag{2.15}$$

In order to use a more compact notation, it is helpful to use the following centered difference notation:

$$\delta_x g(x_i,t) = g(x_{i+\frac{1}{2}},t) - g(x_{i-\frac{1}{2}},t), \tag{2.16}$$

for an arbitrary vector valued function g. Using this notation, Equations (2.14) and (2.15) lead to:

$$\frac{d}{dt}Q_i(t) = -\frac{1}{\Delta x}\delta_x f(q(x_i,t)) \quad \forall i = 1, \cdots, N, \tag{2.17}$$

and

$$Q_i(t_{n+1}) = Q_i(t_n) - \frac{\Delta t}{\Delta x}\delta_x\left(\frac{1}{\Delta t}\int_{t_n}^{t_{n+1}} f(q(x_i,t))\,dt\right), \quad \forall i = 1, \cdots, N, \quad \forall n = 1, \cdots, N_T, \tag{2.18}$$

respectively. It is worth pointing out that we have made no approximation in Equations (2.17) and (2.18). Indeed, if q satisfies Equation (2.2), $\forall [x_1,x_2] \subset [a,b]$ and $\forall t \in [0,T]$, then Equation (2.17) is just Equation (2.2) evaluated in the control volumes and written in terms of the average values Q. Similarly, if q satisfies Equation (2.3), $\forall [x_1,x_2]\times[t_1,t_2] \subset D$, then Equation (2.18) is just Equation (2.3) evaluated in the control volumes, at the time instants

t_n, and written in terms of the average values Q.

Notice that in Equation (2.18) we divided and multiplied by Δt, so that we can interpret $\frac{1}{\Delta t}\int_{t_n}^{t_{n+1}} f(q(x_i,t))\,dt$ as a mean-time average flux. This interpretation is very handy for the derivation of finite-volume schemes.

The formulations given by Equations (2.17) and (2.18) are the cornerstone of the development of finite volume methods for conservation laws. On the right-hand side of Equation (2.17), the flux function f may be discretized leading to an ordinary differential equation (ODE) that might be solved using classical ODE integrators. These methods are known as semi-discrete methods (LeVeque, 2002), since only the spatial coordinate is discretized. In this work we shall restrict our attention to methods based on Equation (2.18).

2.2 The finite-volume approach

We summarize the problem of the system of conservation laws in the integral form discussed in Section 2.1 in Problem 2.1.

Problem 2.1. *Given $D = [a,b]\times[0,T]$, a C^1 flux function $f : \mathbb{R}^m \to \mathbb{R}^m$, $m \geq 1$, we would like to find the weak solution $q \in L^\infty(D,\mathbb{R}^m)$ of the system of conservation laws in the integral form:*

$$\int_{x_1}^{x_2} q(x,t_2)\,dx = \int_{x_1}^{x_2} q(x,t_1)\,dx + \int_{t_1}^{t_2} f(q(x_1,t))\,dt - \int_{t_1}^{t_2} f(q(x_2,t))\,dt,$$

$\forall [x_1,x_2]\times[t_1,t_2] \subset D$, given the initial condition $q(x,0) = q_0(x)$, $\forall x \in [a,b]$, and assuming periodic boundary conditions, i.e., $q(a,t) = q(b,t)$, $\forall t \in [0,T]$.

We point out that, for Problem 2.1, the total mass in $[a,b]$ satisfies:

$$M_{[a,b]}(t) = M_{[a,b]}(0), \quad \forall t \in [0,T]. \tag{2.19}$$

This is the conservation of total mass propriety and is highly desirable for any numerical scheme that intends to give a robust approximation of the system of conservation laws solution.

In Section 2.1 we introduced a version of Problem 2.1 considering a discretization of the domain D. This idea is summarized in Problem 2.2.

Problem 2.2. *Assume the framework of Problem 2.1. We consider positive integers N and N_T, a spatial discretization of [a,b] given by $X_i = [x_{i-\frac{1}{2}}, x_{i+\frac{1}{2}}]$, $\forall i = 1,\cdots,N$, $a = x_{\frac{1}{2}} < x_{\frac{3}{2}} < \cdots < x_{N-\frac{1}{2}} < x_{N+\frac{1}{2}} = b$, $\Delta x = x_{i+\frac{1}{2}} - x_{i-\frac{1}{2}}$, a time discretization $t_n = n\Delta t$, $\Delta t = \frac{T}{N_T}$, $\forall n = 1,\cdots,N_T$. Since we are in the framework of Problem 2.1, it follows that:*

$$Q_i(t_{n+1}) = Q_i(t_n) - \frac{\Delta t}{\Delta x}\delta_x\left(\frac{1}{\Delta t}\int_{t_n}^{t_{n+1}} f(q(x_i,t))\,dt\right), \quad \forall i = 1,\cdots,N, \quad \forall n = 1,\cdots,N_T-1,$$

where $Q_i(t) = \frac{1}{\Delta x}\int_{x_{i-\frac{1}{2}}}^{x_{i+\frac{1}{2}}} q(x,t)\,dx$.

Our problem now consists of finding the values $Q_i(t_n)$, $\forall i = 1, \cdots, N$, $\forall n = 1, \cdots, N_T$, *given the initial values* $Q_i(0)$, $\forall i = 1, \cdots N$. *In other words, we would like to find the average values of* q *in each control volume* X_i *at the considered time instants.*

Finally, we define the one-dimensional (1D) finite-volume (FV) scheme problem as follows in Problem 2.3. We use the notation $q_i^n = q(x_i, t_n)$ to represent the values of q on the discretization of domain D and $u_{i+\frac{1}{2}}^n = u(x_{i+\frac{1}{2}}, t_n)$ to represent the velocity at the control volume edges.

Problem 2.3 (1D-FV scheme)**.** *Assume the framework defined in Problem 2.2. The finite-volume approach of Problem 2.2 consists of a finding a scheme of the form:*

$$Q_i^{n+1} = Q_i^n - \frac{\Delta t}{\Delta x}\delta_i F_i^n, \quad \forall i = 1, \cdots, N, \quad \forall n = 0, \cdots, N_T - 1,$$

where $\delta_i F_i^n = F_{i+\frac{1}{2}}^n - F_{i-\frac{1}{2}}^n$ *and* $Q_i^n \in \mathbb{R}^m$ *is intended to be an approximation of* $Q_i(t_n)$ *in some sense. We define by* $Q_i^0 = Q_i(0)$ *or* $Q_i^0 = q_i^0$. *The term* $F_{i+\frac{1}{2}}^n = \mathcal{F}(Q^n, u^n; i)$, *is known as numerical flux, where* $\mathcal{F}$ *is the numerical flux function, and it approximates* $\frac{1}{\Delta t}\int_{t_n}^{t_{n+1}} f(q(x_{i+\frac{1}{2}}, t))\, dt$, $\forall i = 0, 1, \cdots, N$, *or, in other words, it estimates the time-averaged fluxes at the control volume* X_i *boundaries.*

Notice that in the previous problem, we are using the notations $Q^n = (Q_1^n, \cdots, Q_N^n)$, $u^n = (u_{\frac{1}{2}}^n, \cdots, u_{N+\frac{1}{2}}^n)$

To be written: definitions of convergence, consistency and stability.

2.3 The Piecewise-Parabolic Method

In this Section, we are going to review and analyse the Piecewise-Parabolic method (PPM). This method was proposed by Colella and Woodward (1984) for gas dynamic simulations and its viability for atmospheric simulations has been shown by Carpenter et al. (1990). This method is based in using parabolas to reconstruct the function from its average values, ensuring mass conservation and monotonicity. PPM is an extension of the Piecesiwe-Linear method from Van Leer (1977) and it is employed in the FV3 model using the dimension splitting method from Lin and Rood (1996). This section is organized as follows: in Subsection 2.3.1 we present and analyse the PPM reconstrucion method and the monotonization and flux computation are presented and analysed in Subsections 2.3.2 and 2.3.3, respectively.

2.3.1 Reconstruction

Let us consider a function $q \in L^\infty([a, b], \mathbb{R})$, a discretization of $[a, b]$ as in Problem 2.2 and assume that we are given the average values $Q_i = \frac{1}{\Delta x}\int_{x_{i-\frac{1}{2}}}^{x_{i+\frac{1}{2}}} q(x)\, dx$ on each control volume X_i, $\forall i = 1, \cdots, N$. We make use of the indicator function of each control volume X_i defined by:

$$\chi_i(x) = \begin{cases} 1 & \text{if } x \in X_i \\ 0 & \text{otherwise} \end{cases} \tag{2.20}$$

Our task is to find a piecewise-parabolic (PP) function:

$$q_{PP}(x) = \sum_{i=1}^{N} \chi_i(x) q_i(x), \tag{2.21}$$

where $q_i \in \mathcal{P}_2$ [2] is such that:

1. $\frac{1}{\Delta x} \int_{x_{i-\frac{1}{2}}}^{x_{i+\frac{1}{2}}} q_i(x)\, dx = Q_i$, that is, q_i preserves the mass on each control volume X_i;
2. No new extreme is generated

We shall assume that each q_i may be expressed as:

$$q_i(x) = q_{L,i} + z_i(x)(\Delta q_i + q_{6,i}(1 - z_i(x))), \quad \text{where } z_i(x) = \frac{x - x_{i-\frac{1}{2}}}{\Delta x}, \quad x \in X_i, \tag{2.22}$$

where the values $q_{L,i}$, Δq_i and $q_{6,i}$ will be specified latter. Note that each z_i is just a normalization function that maps X_i onto $[0, 1]$. Under this assumption, it is easy to see that $\lim_{x \to x^+_{i-\frac{1}{2}}} q_i(x) = q_{L,i}$. If we define $q_{R,i} = \lim_{x \to x^-_{i+\frac{1}{2}}} q_i(x)$, then we have:

$$\Delta q_i = q_{R,i} - q_{L,i}. \tag{2.23}$$

The average value of q_i is given by:

$$\frac{1}{\Delta x} \int_{x_{i-\frac{1}{2}}}^{x_{i+\frac{1}{2}}} q_i(x)\, dx = \frac{(q_{L,i} + q_{R,i})}{2} + \frac{q_{6,i}}{6} \tag{2.24}$$

Under the hypothesis of mass conservation, we have:

$$q_{6,i} = 6\left(Q_i - \frac{(q_{L,i} + q_{R,i})}{2}\right). \tag{2.25}$$

Therefore, we have found the parameters Δq_i and $q_{6,i}$ as functions of the parameters $q_{L,i}$ and $q_{R,i}$, such that the polynomial p_i from (2.21) guarantees mass conservation. To completely determine the polynomial p_i, we need to set the values $q_{L,i}$ and $q_{R,i}$, which, as we have seen, represent the limits of q_i when x tends to the left and right boundaries of X_i, respectively. Hence, it is natural to seek for $q_{L,i}$ as an approximation of $q(x_{i-\frac{1}{2}})$ and $q_{R,i}$ as an approximation of $q(x_{i+\frac{1}{2}})$. So, let us describe a way to approximate $q(x_{i+\frac{1}{2}})$, and denote its estimation by $q_{i+\frac{1}{2}}$ $\forall i = 0, 1, \cdots, N$. We introduce the following function:

$$Q(x) = \int_a^x q(\xi)\, d\xi, \tag{2.26}$$

and we notice that:

$$Q(x_{i+\frac{1}{2}}) = \Delta x \sum_{k=1}^{i} Q_k \text{ and } Q'(x) = q(x, t_n). \tag{2.27}$$

[2] $\mathcal{P}_n$ stands for the space of real polynomials of degree $\leq$ n.

Therefore $Q'(x_{i+\frac{1}{2}}) = q(x_{i+\frac{1}{2}})$, $\forall i = 0, 1, \cdots, N$. We introduce a quartic polynomial $Q_{i4} \in \mathcal{P}_4$ that interpolates the data $\left(x_{i+k+\frac{1}{2}}, Q(x_{i+k+\frac{1}{2}})\right)_{k=-2,-1,0,1,2}$. Then, we define $q_{i+\frac{1}{2}} = \frac{d}{dx}Q_{i4}(x_{i+k+\frac{1}{2}})$. An explicit expression for $q_{i+\frac{1}{2}}$ is given by (Colella & Woodward, 1984):

$$q_{i+\frac{1}{2}} = \frac{1}{2}\Big(Q_{i+1} + Q_i\Big) - \frac{1}{6}\Big(\delta Q_{i+1} - \delta Q_i\Big), \tag{2.28}$$

where δQ_i is the average slope in the i-th control-volume:

$$\delta Q_i = \frac{1}{2}\Big(Q_{i+1} - Q_{i-1}\Big). \tag{2.29}$$

We notice that Formula (2.29) may be rewritten more explicitly as:

$$q_{i+\frac{1}{2}} = \frac{7}{12}\Big(Q_{i+1} + Q_i\Big) - \frac{1}{12}\Big(Q_{i+2} + Q_{i-1}\Big). \tag{2.30}$$

The Formula (2.30) is fourth-order accurate if q is at least $\mathcal{C}^4$ (Colella & Woodward, 1984). Indeed, we prove this later in Proposition 2.1 by noticing that this Formula may be thought as a finite-difference scheme. An explicit expression for the values of $q_{R,i}$ and $q_{L,i}$ are given by:

$$q_{R,i} = q_{i+\frac{1}{2}} = \frac{7}{12}\Big(Q_{i+1} + Q_i\Big) - \frac{1}{12}\Big(Q_{i+2} + Q_{i-1}\Big), \tag{2.31}$$

$$q_{L,i} = q_{i-\frac{1}{2}} = \frac{7}{12}\Big(Q_i + Q_{i-1}\Big) - \frac{1}{12}\Big(Q_{i+1} + Q_{i-2}\Big). \tag{2.32}$$

PPM reconstruction numerical analysis

As we pointed out before, the approximation of q at the control volumes edges given by Equation (2.30) is fourth-order accurate when $q \in \mathcal{C}^4([a,b])$. This is proved as corollary of the following Proposition 2.1.

Proposition 2.1. *Let $q \in \mathcal{C}^4([a,b])$, $\overline{x} \in]a,b[$ and $h > 0$ such that $[\overline{x} - 2h, \overline{x} + 2h] \subset [a,b]$. Then, the following identity holds:*

$$q(\overline{x}) = \frac{7}{12}\left(\frac{1}{h}\int_{\overline{x}}^{\overline{x}+h} q(x)\,dx + \frac{1}{h}\int_{\overline{x}-h}^{\overline{x}} q(x)\,dx\right) - \frac{1}{12}\left(\frac{1}{h}\int_{\overline{x}+h}^{\overline{x}+2h} q(x)\,dx + \frac{1}{h}\int_{\overline{x}-2h}^{\overline{x}-h} q(x)\,dx\right) + Ch^4, \tag{2.33}$$

where C is a constant that depends on q and h.

Proof. We define $Q(x) = \int_a^x q(\xi)\,d\xi$ for $x \in [a,b]$ as in Equation (2.26). It follows that:

$$\int_{\overline{x}}^{\overline{x}+h} q(\xi)\,d\xi + \int_{\overline{x}-h}^{\overline{x}} q(\xi)\,d\xi = Q(\overline{x}+h) - Q(\overline{x}-h),$$
$$\int_{\overline{x}+h}^{\overline{x}+2h} q(\xi)\,d\xi + \int_{\overline{x}-2h}^{\overline{x}-h} q(\xi)\,d\xi = Q(\overline{x}+2h) - Q(\overline{x}-2h) - (Q(\overline{x}+h) - Q(\overline{x}-h)).$$

Using these identities, Equation (2.33) may be rewritten as:

$$q(\overline{x}) = \frac{4}{3}\left(\frac{Q(\overline{x}+h) - Q(\overline{x}-h)}{2h}\right) - \frac{1}{3}\left(\frac{Q(\overline{x}+2h) - Q(\overline{x}-2h)}{4h}\right) + Ch^4, \tag{2.34}$$

which consists of finite-difference approximations. Thus, Equation (2.33) follows from Lemma A.1 with:

$$C = \frac{1}{240}\left(q^{(4)}(\theta_h) + q^{(4)}(\theta_{-h})\right) - \frac{1}{45}\left(q^{(4)}(\theta_{2h}) + q^{(4)}(\theta_{-2h})\right), \tag{2.35}$$

where $\theta_h \in [\overline{x}, \overline{x}+h], \theta_{-h} \in [\overline{x}-h, \overline{x}], \theta_{2h} \in [\overline{x}, \overline{x}+2h], \theta_{-2h} \in [\overline{x}-2h, \overline{x}]$, which concludes the proof.

Corollary 2.1. *It follows from Proposition 2.1 with* $\overline{x} = x_{i+\frac{1}{2}}$ *and* $h = \Delta x$ *that* $q_{i+\frac{1}{2}}$ *given by Equation* (2.30) *satisfies:*

$$q(x_{i+\frac{1}{2}}) - q_{i+\frac{1}{2}} = C\Delta x^4, \tag{2.36}$$

with C *given by right-hand side of Equation* (2.35)*. Besides that, we also have the following bound:*

$$\left|q(x_{i+\frac{1}{2}}) - q_{i+\frac{1}{2}}\right| \leq C_1 \Delta x^4, \tag{2.37}$$

where:

$$C_1 = \frac{19}{360} \sup_{x\in[a,b]} |q^{(4)}(x)|, \tag{2.38}$$

is a constant that depends only on q*.*

The parabolic function from (2.33) given with coefficients specified before approximates q with order 3 when $q \in C^4([a,b])$. In order to check this, for $x \in X_i$ we rewrite Equation (2.22) as:

$$q_i(x) = q_{L,i} + \frac{(\Delta q_i + q_{6,i})}{\Delta x}(x - x_{i-\frac{1}{2}}) - \frac{q_{6,i}}{(\Delta x)^2}(x - x_{i-\frac{1}{2}})^2 \tag{2.39}$$

and we write q using its Taylor expansion assuming $q \in C^4([a,b])$:

$$q(x) = q(x_{i-\frac{1}{2}}) + q'(x_{i-\frac{1}{2}})(x - x_{i-\frac{1}{2}}) + \frac{q''(x_{i-\frac{1}{2}})}{2}(x - x_{i-\frac{1}{2}})^2 + \frac{q^{(3)}(\theta_i)}{6}(x - x_{i-\frac{1}{2}})^3, \tag{2.40}$$

where $\theta_i \in X_i$. Comparing Equation (2.39) with Equation (2.40), it is reasonable to seek to

some bound to the expressions:

$$q'(x_{i-\frac{1}{2}}) - \frac{(\Delta q_i + q_{6,i})}{\Delta x}, \tag{2.41}$$

and:

$$\frac{q''(x_{i-\frac{1}{2}})}{2} - \left(- \frac{q_{6,i}}{(\Delta x)^2} \right). \tag{2.42}$$

We have seen that term $q_{L,i}$ gives a fourth-order approximation to $q(x_{i-\frac{1}{2}})$. The Corollary 2.2 shall prove that the term (2.41) has a bound proportional to $(\Delta x)^2$, and the Corollary 2.3 shall prove that the term (2.42) is bounded by a constant times Δx.

Before proving finding the desired bounds, it is useful to rewrite some terms explicitly as functions of the values Q_i's. Combining Equation (2.25) with Equations (2.31) and (2.32), we may write $q_{6,i}$ as:

$$q_{6,i} = \frac{1}{4}\left(Q_{i-2} - 6Q_{i-1} + 10Q_i - 6Q_{i+1} + Q_{i+2} \right). \tag{2.43}$$

Recalling the definition of Δq_i from Equation (2.23), and applying Equations (2.31) and (2.32), we may express Δq_i as:

$$\Delta q_i = \frac{1}{12}\left(Q_{i-2} - 8Q_{i-1} + 8Q_{i+1} - Q_{i+2} \right). \tag{2.44}$$

Finally, we combine Equations (2.43) and (2.44) and write their sum as:

$$\frac{(\Delta q_i + q_{6,i})}{\Delta x} = \frac{2Q_{i-2} - 13Q_{i-1} + 15Q_i - 5Q_{i+1} + Q_{i+2}}{6\Delta x}. \tag{2.45}$$

The next Proposition 2.2 proves that Equation (2.45) approximates $q'(x_{i-\frac{1}{2}})$ with order 2.

Proposition 2.2. *Let $q \in C^3([a,b])$, $\overline{x} \in]a,b[$, and $h > 0$ such that $[\overline{x} - 2h, \overline{x} + 3h] \subset [a,b]$ Then, the following identity holds:*

$$\begin{aligned} q'(\overline{x}) = \frac{1}{6h}\Bigg(& \frac{2}{h}\int_{\overline{x}-2h}^{\overline{x}-h} q(x)\,dx - \frac{13}{h}\int_{\overline{x}-h}^{\overline{x}} q(x)\,dx + \frac{15}{h}\int_{\overline{x}}^{\overline{x}+h} q(x)\,dx \\ & - \frac{5}{h}\int_{\overline{x}+h}^{\overline{x}+2h} q(x)\,dx + \frac{1}{h}\int_{\overline{x}+2h}^{\overline{x}+3h} q(x)\,dx \Bigg) + Ch^2, \end{aligned} \tag{2.46}$$

where C is a constant that depends on q and h.

Proof. We consider again $Q(x) = \int_a^x q(\xi)\,d\xi$ for $x \in [a,b]$ as in Equation (2.26). Like in

Proposition 2.2, we have:

$$\begin{aligned}\frac{1}{6h}\left(\frac{2}{h}\int_{\overline{x}-2h}^{\overline{x}-h} q(x)\,dx - \frac{13}{h}\int_{\overline{x}-h}^{\overline{x}} q(x)\,dx + \frac{15}{h}\int_{\overline{x}}^{\overline{x}+h} q(x)\,dx - \frac{5}{h}\int_{\overline{x}+h}^{\overline{x}+2h} q(x)\,dx + \frac{1}{h}\int_{\overline{x}+2h}^{\overline{x}+3h} q(x)\,dx\right)\\ = \frac{1}{6h}\left(\frac{2}{h}\big(Q(\overline{x}-h)-Q(\overline{x}-2h)\big) - \frac{13}{h}\big(Q(\overline{x})-Q(\overline{x}-h)\big) + \frac{15}{h}\big(Q(\overline{x}+h)-Q(\overline{x})\big)\right.\\ \left. -\frac{5}{h}\big(Q(\overline{x}+2h)-Q(\overline{x}+h)\big) + \frac{1}{h}\big(Q(\overline{x}+3h)-Q(\overline{x}+2h)\big)\right)\\ = \frac{1}{6h^2}\Big(-2Q(\overline{x}-2h)+15Q(\overline{x}-h)-28Q(\overline{x})+20Q(\overline{x}+h)-6Q(\overline{x}+2h)+Q(\overline{x}+3h)\Big),\end{aligned}$$

which consists of the finite-difference scheme from Lemma A.2. Therefore, Equation (2.46) follows from Lemma A.2 with:

$$C = \frac{1}{24}\Big(32q^{(3)}(\theta_{-2h}) - 15q^{(3)}(\theta_{-h}) - 20q^{(3)}(\theta_h) + 96q^{(3)}(\theta_{2h}) - 81q^{(3)}(\theta_{3h})\Big), \tag{2.47}$$

where $\theta_h \in [\overline{x}, \overline{x}+h]$, $\theta_{-h} \in [\overline{x}-h, \overline{x}]$, $\theta_{2h} \in [\overline{x}, \overline{x}+2h]$, $\theta_{-2h} \in [\overline{x}-2h, \overline{x}]$, $\theta_{3h} \in [\overline{x}, \overline{x}+3h]$, which concludes the proof.

Corollary 2.2. *It follows from Proposition 2.2 with* $\overline{x} = x_{i-\frac{1}{2}}$ *and* $h = \Delta x$ *that* Δq_i *given by Equation* (2.44) *and* $q_{6,i}$ *given by Equation* (2.43) *satisfy:*

$$q'(x_{i-\frac{1}{2}}) - \frac{(\Delta q_i + q_{6,i})}{\Delta x} = C\Delta x^2, \tag{2.48}$$

with C *given by right-hand side of Equation* (2.47)*. Besides that, we also have the following bound:*

$$\left|q'(x_{i-\frac{1}{2}}) - \frac{(\Delta q_i + q_{6,i})}{\Delta x}\right| \leq C_2\Delta x^2, \tag{2.49}$$

where:

$$C_2 = \frac{244}{24}\sup_{x\in[a,b]}|q^{(3)}(x)| \tag{2.50}$$

is a constant that depends only on q*.*

Now, we analyse the following expression:

$$-\frac{2q_{6,i}}{\Delta x^2} = -\frac{1}{2\Delta x^2}\Big(Q_{i-2} - 6Q_{i-1} + 10Q_i - 6Q_{i+1} + Q_{i+2}\Big). \tag{2.51}$$

deduced from Equation (2.43) and we prove in Proposition 2.3 that Equation (2.51) approximates $q''(x_{i-\frac{1}{2}})$ with order 1.

Proposition 2.3. *Let* $q \in C^3([a,b])$, $\overline{x} \in]a,b[$ *and* $h > 0$ *such that* $[\overline{x}-2h, \overline{x}+3h] \subset [a,b]$.

Then, the following identity holds:

$$q''(\overline{x}) = \frac{1}{2h^2}\left(-\frac{1}{h}\int_{\overline{x}-2h}^{\overline{x}-h} q(x)\,dx + \frac{6}{h}\int_{\overline{x}-h}^{\overline{x}} q(x)\,dx - \frac{10}{h}\int_{\overline{x}}^{\overline{x}+h} q(x)\,dx + \frac{6}{h}\int_{\overline{x}+h}^{\overline{x}+2h} q(x)\,dx - \frac{1}{h}\int_{\overline{x}+2h}^{\overline{x}+3h} q(x)\,dx\right) + Ch, \tag{2.52}$$

where C is a constant that depends on q and h.

Proof. Similarly to Proposition 2.2 using the same function Q, we have:

$$\begin{aligned}
&\frac{1}{2h^2}\left(-\frac{1}{h}\int_{\overline{x}-2h}^{\overline{x}-h} q(x)\,dx + \frac{6}{h}\int_{\overline{x}-h}^{\overline{x}} q(x)\,dx - \frac{10}{h}\int_{\overline{x}}^{\overline{x}+h} q(x)\,dx + \frac{6}{h}\int_{\overline{x}+h}^{\overline{x}+2h} q(x)\,dx - \frac{1}{h}\int_{\overline{x}+2h}^{\overline{x}+3h} q(x)\,dx\right) \\
&\quad = \frac{1}{2h^2}\left(-\frac{1}{h}\big(Q(\overline{x}-h) - Q(\overline{x}-2h)\big) + \frac{6}{h}\big(Q(\overline{x}) - Q(\overline{x}-h)\big) - \frac{10}{h}\big(Q(\overline{x}+h) - Q(\overline{x})\big)\right. \\
&\qquad \left. + \frac{6}{h}\big(Q(\overline{x}+2h) - Q(\overline{x}+h)\big) - \frac{1}{h}\big(Q(\overline{x}+3h) - Q(\overline{x}+2h)\big)\right) \\
&\quad = \frac{1}{2h^3}\Big(Q(\overline{x}-2h) - 7Q(\overline{x}-h) + 16Q(\overline{x}) - 16Q(\overline{x}+h) + 7Q(\overline{x}+2h) - Q(\overline{x}+3h)\Big),
\end{aligned}$$

which consists of the finite-difference scheme from Lemma A.3. Therefore, Equation (2.52) follows from Lemma A.3 with:

$$C = \frac{1}{48}\left(-16q^{(3)}(\theta_{-2h}) + 7q^{(3)}(\theta_{-h}) + 16q^{(3)}(\theta_h) - 112q^{(3)}(\theta_{2h}) + 81q^{(3)}(\theta_{3h})\right), \tag{2.53}$$

where $\theta_h \in [\overline{x}, \overline{x}+h], \theta_{-h} \in [\overline{x}-h, \overline{x}]$, $\theta_{2h} \in [\overline{x}, \overline{x}+2h], \theta_{-2h} \in [\overline{x}-2h, \overline{x}]$, $\theta_{3h} \in [\overline{x}, \overline{x}+3h]$, which concludes the proof.

Corollary 2.3. *It follows from Proposition 2.3 with $\overline{x} = x_{i-\frac{1}{2}}$ and $h = \Delta x$ that $q_{6,i}$ given by Equation (2.30) satisfies:*

$$q''(x_{i-\frac{1}{2}}) - \left(-\frac{2q_{6,i}}{(\Delta x)^2}\right) = C\Delta x, \tag{2.54}$$

with C given by right-hand side of Equation (2.53). Besides that, we also have the following bound:

$$\left|\frac{q''(x_{i-\frac{1}{2}})}{2} - \left(-\frac{q_{6,i}}{(\Delta x)^2}\right)\right| \leq C_3\Delta x, \tag{2.55}$$

where:

$$C_3 = \frac{232}{96}\sup_{x\in[a,b]} |q^{(3)}(x)| \tag{2.56}$$

is a constant that depends only on q.

With the aid of Corollaries 2.1, 2.2, and 2.3, we are able to prove that the PPM reconstruction approximates q with order 3. Indeed, we prove this on the follow up Proposition 2.4.

Proposition 2.4. *Let $q \in C^4([a,b])$. Then, the piecewise parabolic function given by Equation (2.22) with the parameters $q_{R,i}$ and $q_{L,i}$ obeying Equations (2.31) and (2.32) gives a third-order aproximation to q on the control volume X_i.*

Proof. For $x \in X_i$, from Equations (2.40) and (2.39), we have:

$$q(x) - q_i(x) = (q'(x_{i-\frac{i}{2}}) - q_{L,i}) + \left(q'(x_{i-\frac{1}{2}}) - \frac{(\Delta q_i + q_{6,i})}{\Delta x}\right)(x - x_{i-\frac{1}{2}}) + \left(\frac{q''(x_{i-\frac{1}{2}})}{2} + \frac{q_{6,i}}{(\Delta x)^2}\right)(x - x_{i-\frac{1}{2}})^2 + \frac{q^{(3)}(\theta_i)}{6}(x - x_{i-\frac{1}{2}})^3.$$

For $x \in X_i$, we have $|x - x_{i-\frac{i}{2}}| \leq \Delta x$. Using this fact with Corollaries 2.1, 2.2, and 2.3, we have:

$$\begin{aligned} |q(x) - q_i(x)| &\leq |q'(x_{i-\frac{i}{2}}) - q_{L,i}| + \left|q'(x_{i-\frac{1}{2}}) - \frac{(\Delta q_i + q_{6,i})}{\Delta x}\right||x - x_{i-\frac{1}{2}}| \\ &+ \left|\frac{q''(x_{i-\frac{1}{2}})}{2} + \frac{q_{6,i}}{(\Delta x)^2}\right||x - x_{i-\frac{1}{2}}|^2 + \frac{|q^{(3)}(\theta_i)|}{6}|x - x_{i-\frac{1}{2}}|^3 \\ &\leq C_1(\Delta x)^4 + \left(C_2 + C_3 + \frac{1}{6}\sup_{\xi \in [a,b]}|q^{(3)}(\xi)|\right)(\Delta x)^3, \end{aligned}$$

where C_1, C_2 and C_3 are given by Equations (2.38), (2.50) and (2.56), respectively, which concludes the proof.

2.3.2 Monotonization - to be written

2.3.3 Flux

Let us assume the framework from Problem 2.3 for the linear advection equation for a single conservated variable, *i.e.*, $m = 1$ and the flux function $f(q(x,t)) = u(x,t)q(x,t)$, where the velocity function u is given. Supposing that the average grid values $Q^n = (Q_1^n, \cdots, Q_N^n)$ are known, we would like to compute the values Q^{n+1}. This is achieved using a scheme of the type given in Problem 2.3. Therefore, we need to estimate the time-average flux. For each control volume edge $i = 0, \cdots, N$ and $y > 0$ we define the following average of the piecewise-parabolic approximation defined in Equation (2.21) for the data Q^n (Colella & Woodward, 1984):

$$F_{L,i+\frac{1}{2}}(y) = \frac{1}{y}\int_{x_{i+\frac{1}{2}}-y}^{x_{i+\frac{1}{2}}} q_{PP}(\xi)\,d\xi, \tag{2.57}$$

and

$$F_{R,i+\frac{1}{2}}(y) = \frac{1}{y}\int_{x_{i+\frac{1}{2}}}^{x_{i+\frac{1}{2}}+y} q_{PP}(\xi)\,d\xi, \tag{2.58}$$

If $y \leq \Delta x$, then both of the above integral domains are constrained to a single control volume. Thus, it follows from a straightforward computation using Equation (2.22) that:

$$F_{L,i+\frac{1}{2}}(y) = \frac{1}{y}\int_{x_{i+\frac{1}{2}}-y}^{x_{i+\frac{1}{2}}} q_i(\xi)\,d\xi = q_{R,i} + \frac{(q_{6,i} - \Delta q_i)}{2\Delta x}y - \frac{q_{6,i}}{3(\Delta x)^2}y^2, \tag{2.59}$$

and

$$F_{R,i+\frac{1}{2}}(y) = \frac{1}{y}\int_{x_{i+\frac{1}{2}}}^{x_{i+\frac{1}{2}}+y} q_{i+1}(\xi)\,d\xi = q_{L,i+1} + \frac{(q_{6,i+1}+\Delta q_{i+1})}{2\Delta x}y - \frac{q_{6,i+1}}{3(\Delta x)^2}y^2. \tag{2.60}$$

The numerical flux is then defined by:

$$F_{i+\frac{1}{2}}(Q^n) = \begin{cases} u^n_{i+\frac{1}{2}} F_{L,i+\frac{1}{2}}(u^n_{i+\frac{1}{2}}\Delta t) & \text{if } u^n_{i+\frac{1}{2}} \geq 0, \\ u^n_{i+\frac{1}{2}} F_{R,i+\frac{1}{2}}(-u^n_{i+\frac{1}{2}}\Delta t) & \text{if } u^n_{i+\frac{1}{2}} < 0, \end{cases} \tag{2.61}$$

Notice that if we define:

$$c^n_{i+\frac{1}{2}} = u^n_{i+\frac{1}{2}}\frac{\Delta t}{\Delta x}, \tag{2.62}$$

the requirement $y \leq \Delta x$ for Equation (2.61) is equivalent to require that $|c^n_{i+\frac{1}{2}}| \leq 1$ for all i, which is the CFL condition. In the absence of monotonization, it follows from Equations (2.31), (2.32), (2.43) and (2.44) that the numerical flux may be expressed as the following stencil:

$$F_{i+\frac{1}{2}}(Q^n) = \frac{u^n_{i+\frac{1}{2}}}{12}\left(\alpha_i Q^n_{i-2} + \beta_i Q^n_{i-1} + \gamma_i Q^n_i + \delta_i Q^n_{i+1} + \epsilon_i Q^n_{i+2} + \zeta_i Q^n_{i+3}\right), \tag{2.63}$$

where the coefficients are given by:

$$\alpha_i = \begin{cases} c_{i+\frac{1}{2}} - c^2_{i+\frac{1}{2}} & \text{if } u^n_{i+\frac{1}{2}} \geq 0, \\ 0 & \text{if } u^n_{i+\frac{1}{2}} < 0, \end{cases} \tag{2.64}$$

$$\beta_i = \begin{cases} -1 - 5c_{i+\frac{1}{2}} + 6c^2_{i+\frac{1}{2}} & \text{if } u^n_{i+\frac{1}{2}} \geq 0, \\ -1 + 2c_{i+\frac{1}{2}} - c^2_{i+\frac{1}{2}} & \text{if } u^n_{i+\frac{1}{2}} < 0, \end{cases} \tag{2.65}$$

$$\gamma_i = \begin{cases} 7 + 15c_{i+\frac{1}{2}} - 10c^2_{i+\frac{1}{2}} & \text{if } u^n_{i+\frac{1}{2}} \geq 0, \\ 7 - 13c_{i+\frac{1}{2}} + 6c^2_{i+\frac{1}{2}} & \text{if } u^n_{i+\frac{1}{2}} < 0, \end{cases} \tag{2.66}$$

$$\delta_i = \begin{cases} 7 - 13c_{i+\frac{1}{2}} + 6c^2_{i+\frac{1}{2}} & \text{if } u^n_{i+\frac{1}{2}} \geq 0, \\ 7 + 15c_{i+\frac{1}{2}} - 10c^2_{i+\frac{1}{2}} & \text{if } u^n_{i+\frac{1}{2}} < 0, \end{cases} \tag{2.67}$$

$$\epsilon_i = \begin{cases} -1 + 2c_{i+\frac{1}{2}} - c^2_{i+\frac{1}{2}} & \text{if } u^n_{i+\frac{1}{2}} \geq 0, \\ -1 - 5c_{i+\frac{1}{2}} + 6c^2_{i+\frac{1}{2}} & \text{if } u^n_{i+\frac{1}{2}} < 0, \end{cases} \tag{2.68}$$

$$\zeta_i = \begin{cases} 0 & \text{if } u^n_{i+\frac{1}{2}} \geq 0, \\ c_{i+\frac{1}{2}} - c^2_{i+\frac{1}{2}} & \text{if } u^n_{i+\frac{1}{2}} < 0, \end{cases} \tag{2.69}$$

Flux numerical analysis

To be written!

2.3.4 Numerical experiements - to be written

Chapter 3

Two-dimensional finite-volume methods

3.1 Two-dimensional system of conservation laws in integral form

Let us consider $\mathcal{C}^1$ flux functions $f : \mathbb{R}^m \to \mathbb{R}^m$ and $g : \mathbb{R}^m \to \mathbb{R}^m$ in x and y direction, respectively. A two-dimensional system of conservation laws in the differential form in a domain $\Omega = [a,b] \times [c,d] \subset \mathbb{R}^2$ associated to the fluxes f and g is given by:

$$\frac{\partial}{\partial t} q(x,y,t) + \frac{\partial}{\partial x} f(q(x,y,t)) + \frac{\partial}{\partial y} g(q(x,y,t)) = 0, \quad \forall (x,y,t) \in \Omega^{\circ} \times]0,+\infty[.^{1} \tag{3.1}$$

The solution q is interpreted as the vector of state variable densities. A classical or strong solution to this system of conservation laws is a $\mathcal{C}^1$ function q satisfying Equation (3.1). As we did in Section 2.1, our goal is to deduce an integral form of Equation (3.1). To do so, let us consider $[x_1,x_2] \times [y_1,y_2] \subset \Omega^{\circ}$ and $[t_1,t_2] \subset [0,+\infty[$. Integrating Equation (3.1) over $[x_1,x_2] \times [y_1,y_2]$ yields:

$$\begin{aligned} \frac{d}{dt}\left(\int_{x_1}^{x_2} \int_{y_1}^{y_2} q(x,y,t)\, dx\, dy \right) = &- \int_{y_1}^{y_2} \Big(f(q(x_2,y,t)) - f(q(x_1,y,t)) \Big)\, dy \\ &- \int_{x_1}^{x_2} \Big(g(q(x,y_2,t)) - g(q(x,y_1,t)) \Big)\, dx. \end{aligned} \tag{3.2}$$

Integrating Equation (3.2) over the time interval $[t_1,t_2]$, we have:

[1] Ω° denotes the interior of Ω. Namely, $\Omega^{\circ} =]a,b[\times]c,d[$.

$$\int_{x_1}^{x_2}\int_{y_1}^{y_2} q(x,y,t_{n+1})\,dx\,dy = \int_{x_1}^{x_2}\int_{y_1}^{y_2} q(x,y,t_n)\,dx\,dy - \int_{t_1}^{t_2}\int_{y_1}^{y_2}\Big(f(q(x_2,y,t)) - f(q(x_1,y,t))\Big)\,dy\,dt - \int_{t_1}^{t_2}\int_{x_1}^{x_2}\Big(g(q(x,y_2,t)) - g(q(x,y_1,t))\Big)\,dx\,dt. \tag{3.3}$$

Equation (3.3) is the integral form of Equation (3.1). We say that $q \in L^\infty(\Omega \times [0,+\infty[, \mathbb{R}^m)$ is a weak solution to the system of conservation laws (3.1) if q satisfies the integral form (3.3), $\forall [x_1,x_2]\times[y_1,y_2] \subset \Omega^o$ and $\forall [t_1,t_2] \subset [0,+\infty[$. Similarly to Section 2.1, these problems are equivalent when q is a C^1 function.

We consider an initial condition $q_0 \in L^\infty(\Omega)$, $q(x,y,0) = q_0(x,y)$, $\forall (x,y) \in \Omega$. Boundary conditions will be assumed bi-periodic. At last, the matrix $\alpha Df(q) + \beta Dg(q)$ is assumed to have real eigenvalues and be diagonalizable $\forall q \in \mathbb{R}^m, \forall \alpha,\beta \in \mathbb{R}$ (LeVeque, 1990), so that we have a hyperbolic conservation law. Therefore, we are again dealing with a Cauchy problem.

To move in the direction of a discrete version of Equation (3.3), let us discretize the domain $D = \Omega \times [0,T]$ following the notations of Section 2.1. Given a positive integer N_T, we define the time step $\Delta t = \frac{T}{N_T}$, $t_n = n\Delta t$, for $n = 0,1,\cdots,N_T$. The spatial discretization is constructed through an uniformly spaced partition of Ω given by:

$$[a,b] = \bigcup_{i=1}^{N} X_i, \text{ where } X_i = [x_{i-\frac{1}{2}}, x_{i+\frac{1}{2}}] \text{ and } a = x_{\frac{1}{2}} < x_{\frac{3}{2}} < \cdots < x_{N-\frac{1}{2}} < x_{N+\frac{1}{2}} = b, \tag{3.4}$$

$$[c,d] = \bigcup_{j=1}^{M} Y_j, \text{ where } Y_j = [y_{j-\frac{1}{2}}, y_{j+\frac{1}{2}}] \text{ and } c = y_{\frac{1}{2}} < y_{\frac{3}{2}} < \cdots < y_{M-\frac{1}{2}} < y_{M+\frac{1}{2}} = d, \tag{3.5}$$

$$\Omega = \bigcup_{i=1}^{N}\bigcup_{j=1}^{M} \Omega_{ij}, \text{ where } \Omega_{ij} = X_i \times Y_j. \tag{3.6}$$

The regions Ω_{ij} are known as control volumes. Similarly to Chapter 2 we employ the notations $\Delta x = x_{i+\frac{1}{2}} - x_{i-\frac{1}{2}}$, $\Delta y = y_{j+\frac{1}{2}} - y_{j-\frac{1}{2}}$ and $x_i = \frac{1}{2}(x_{i+\frac{1}{2}} + x_{i-\frac{1}{2}})$ $y_j = \frac{1}{2}(y_{j+\frac{1}{2}} + y_{j-\frac{1}{2}})$, $\forall i = 1,\cdots,N, \forall j = 1,\cdots,M$, to define the control volume lengths and midpoints, respectively. Finally, we denote by $Q_{ij}(t) \in \mathbb{R}^m$ as the vector of average values of state variable vector at time t in the control volume Ω_{ij}, that is:

$$Q_{ij}(t) = \frac{1}{\Delta x \Delta y}\int_{x_{i-\frac{1}{2}}}^{x_{i+\frac{1}{2}}}\int_{y_{j-\frac{1}{2}}}^{y_{j-\frac{1}{2}}} q(x,t)\,dx \in \mathbb{R}^m. \tag{3.7}$$

Substituting t_1, t_2, x_1, x_2, y_1 and y_2 by $t_n, t_{n+1}, x_{i-\frac{1}{2}}, x_{i+\frac{1}{2}}, y_{j-\frac{1}{2}}, y_{j+\frac{1}{2}}$, respectively, in Equa-

tion (3.3), we obtain:

$$Q_{ij}(t_{n+1}) = Q_{ij}(t_n) - \frac{\Delta t}{\Delta x \Delta y}\delta_x\left(\frac{1}{\Delta t}\int_{t_1}^{t_2}\int_{y_{j-\frac{1}{2}}}^{y_{j+\frac{1}{2}}} f(q(x_i, y, t))\,dy\,dt\right) - \frac{\Delta t}{\Delta x \Delta y}\delta_y\left(\frac{1}{\Delta t}\int_{t_1}^{t_2}\int_{x_{i-\frac{1}{2}}}^{x_{i+\frac{1}{2}}} g(q(x, y_j, t))\,dx\,dt\right), \tag{3.8}$$

where we are using the centered finite-difference notation:

$$\delta_x h(x_i, y, t) = h(x_{i+\frac{1}{2}}, y, t) - h(x_{i-\frac{1}{2}}, y, t), \tag{3.9}$$

$$\delta_y h(x, y_j, t) = h(x, y_{j+\frac{1}{2}}, t) - h(x, y_{j-\frac{1}{2}}, t), \tag{3.10}$$

for any function h. The Equation (3.8) is useful to motivate two-dimensional finite-volume schemes, as we shall see in the next section.

3.2 The finite-volume approach

This Section is basically an extension to two dimensions of the concepts presented in Section 2.2. The problem of two-dimensional system of conservation laws in the integral form presented Section 3.1 is written in a concise way in Problem 3.1.

Problem 3.1. *Given $\Omega = [a, b] \times [c, d]$, $D = \Omega \times [0, T]$, C^1 flux functions $f, g : \mathbb{R}^m \to \mathbb{R}^m$, $m \geq 1$, we would like to find the weak solution $q \in L^\infty(D, \mathbb{R}^m)$ of the two-dimensional system of conservation laws in the integral form:*

$$\begin{aligned}\int_{x_1}^{x_2}\int_{y_1}^{y_2} q(x, y, t)\,dx\,dy = &\int_{x_1}^{x_2}\int_{y_1}^{y_2} q(x, y, t)\,dx\,dy \\ &- \int_{t_1}^{t_2}\int_{y_1}^{y_2}\Big(f(q(x_2, y, t)) - f(q(x_1, y, t))\Big)\,dy\,dt \\ &- \int_{t_1}^{t_2}\int_{x_1}^{x_2}\Big(g(q(x, y_2, t)) - g(q(x, y_1, t))\Big)\,dx\,dt.\end{aligned}$$

$\forall [x_1, x_2]\times[y_1, y_2]\times[t_1, t_2] \subset D$, given the initial condition $q(x, y, 0) = q_0(x, y)$, $\forall (x, y) \in \Omega$, and assuming bi-periodic boundary conditions, i.e., $q(a, y, t) = q(b, y, t)$, $\forall t \in [0, T]$, $\forall y \in [c, d]$, and $q(x, c, t) = q(x, d, t)$, $\forall t \in [0, T]$, $\forall x \in [a, b]$.

For Problem 3.1, the total mass in Ω is defined by:

$$M_\Omega(t) = \int_\Omega q(x, y, t)\,dx\,dy \in \mathbb{R}^m, \quad \forall t \in [0, T], \tag{3.11}$$

and is conserved within time:

$$M_\Omega(t) = M_\Omega(0), \quad \forall t \in [0, T]. \tag{3.12}$$

Section 3.1 introduced a version of Problem 3.1 considering a discretization of the

domain D. This version is also summarized in Problem 3.2.

Problem 3.2. *Assume the framework of Problem 3.1. We consider positive integers N and N_T, a spatial discretization of [a,b] given by $X_i = [x_{i-\frac{1}{2}}, x_{i+\frac{1}{2}}]$, $\forall i = 1, \cdots, N$, $a = x_{\frac{1}{2}} < x_{\frac{3}{2}} < \cdots < x_{N-\frac{1}{2}} < x_{N+\frac{1}{2}} = b$, $\Delta x = x_{i+\frac{1}{2}} - x_{i-\frac{1}{2}}$, $Y_j = [y_{j-\frac{1}{2}}, y_{j+\frac{1}{2}}]$, $\forall j = 1, \cdots, M$, $c = y_{\frac{1}{2}} < y_{\frac{3}{2}} < \cdots < y_{M-\frac{1}{2}} < y_{M+\frac{1}{2}} = d$, $\Delta y = y_{j+\frac{1}{2}} - y_{j-\frac{1}{2}}$, $\Omega_{ij} = X_i \times Y_j$, a time discretization $t_n = n\Delta t$, $\Delta t = \frac{T}{N_T}$, $\forall n = 1, \cdots, N_T$. Since we are in the framework of Problem 3.2, it follows that:*

$$Q_{ij}(t_{n+1}) = Q_{ij}(t_n) - \frac{\Delta t}{\Delta x \Delta y}\delta_x\left(\frac{1}{\Delta t}\int_{t_1}^{t_2}\int_{y_{j-\frac{1}{2}}}^{y_{j+\frac{1}{2}}} f(q(x_i, y, t))\,dy\,dt\right) - \frac{\Delta t}{\Delta x \Delta y}\delta_y\left(\frac{1}{\Delta t}\int_{t_1}^{t_2}\int_{x_{i-\frac{1}{2}}}^{x_{i+\frac{1}{2}}} g(q(x, y_j, t))\,dx\,dt\right),$$

where $Q_{ij}(t) = \frac{1}{\Delta x \Delta y}\int_{x_{i-\frac{1}{2}}}^{x_{i+\frac{1}{2}}}\int_{y_{j-\frac{1}{2}}}^{y_{j+\frac{1}{2}}} q(x, y, t)\,dx\,dy$.

Our problem now consists of finding the values $Q_{ij}(t_n)$, $\forall i = 1, \cdots, N$, $\forall j = 1, \cdots, M$, $\forall n = 1, \cdots, N_T$, given the initial values $Q_{ij}(0)$, $\forall i = 1, \cdots N$, $\forall j = 1, \cdots, M$. In other words, we would like to find the average values of q in each control volume Ω_{ij} at the considered time instants.

Finally, we define the one-dimensional (2D) finite-volume (FV) scheme problem as follows in Problem 3.3. We use the notation $q_{ij}^n = q(x_i, y_j, t_n)$ to represent the values of q in the discrete domain D and $u_{i+\frac{1}{2},j}^n = u(x_{i+\frac{1}{2}}, y_j, t_n)$ to represent the velocity in x direction at control volume edges midpoints in the x direction, and $v_{i,j+\frac{1}{2}}^n = v(x_i, y_{j+\frac{1}{2}}, t_n)$ to represent the velocity in y direction at control volume edges midpoints in the y direction,

Problem 3.3 (2D-FV scheme)**.** *Assume the framework defined in Problem 3.2. The finite-volume approach of Problem 3.1 consists of a finding a scheme of the form:*

$$Q_{ij}^{n+1} = Q_{ij}^n - \frac{\Delta t}{\Delta x \Delta y}\delta_i F_{i,j}^n - \frac{\Delta t}{\Delta x \Delta y}\delta_j G_{i,j}^n,$$
$$\forall i = 1, \cdots, N, \quad \forall j = 1, \cdots, M, \quad \forall n = 1, \cdots, N_T - 1,$$

where $\delta_i F_{ij}^n = F_{i+\frac{1}{2},j}^n - F_{i-\frac{1}{2},j}^n$, $\delta_j G_{ij}^n = G_{i,j+\frac{1}{2}}^n - G_{i,j-\frac{1}{2}}^n$ and $Q_{ij}^n \in \mathbb{R}^m$ is intended to be an approximation of $Q_{ij}(t_n)$ in some sense. We define by $Q_{ij}^0 = Q_{ij}(0)$ or $Q_{ij}^0 = q_{i,j}^0$.

The term $F_{i+\frac{1}{2},j}^n = \mathcal{F}(Q^n; u^n; i, j)$ is known as numerical flux in the x direction, where $\mathcal{F}$ is the numerical flux function, and it approximates $\frac{1}{\Delta t}\int_{t_n}^{t_{n+1}}\int_{y_{j-\frac{1}{2}}}^{y_{j+\frac{1}{2}}} f(q(x_{i+\frac{1}{2}}, y, t))\,dy\,dt$, $\forall i = 0, 1, \cdots, N$, and $G_{i,j+\frac{1}{2}}^n = \mathcal{G}(Q^n, v^n; i, j)$ is known as numerical flux in the y direction, where $\mathcal{G}$ is the numerical flux function, and it approximates $\frac{1}{\Delta t}\int_{t_n}^{t_{n+1}}\int_{x_{i-\frac{1}{2}}}^{x_{i+\frac{1}{2}}} g(q(x, y_{j+\frac{1}{2}}, t))\,dx\,dt$, $\forall j = 0, 1, \cdots, M$, or, in other words, they estimate the time-averaged fluxes at the control volume Ω_{ij} boundaries.

$Q^n = (Q_{ij}^n)_{i=1,\cdots,N, j=1,\cdots,M}$

3.3 Dimension splitting

(Lin & Rood, 1997) (Lin, 2004) (Putman, 2007) (Putman & Lin, 2007)

Chapter 4

Cubed-sphere grids

(Sadourny, 1972) (Ronchi et al., 1996) (Rančić et al., 1996) (Taylor et al., 1997) (Nair et al., 2005) (Lauritzen et al., 2011)

To be written!

4.1 Equidistant cubed-sphere

We consider a radius $R > 0$ and $a = \frac{R}{\sqrt{3}}$ representing the half-length of the cube, and the family of maps $\Psi_p : [-a, a] \times [-a, a] \to \mathbb{S}^2_R$, $p = 1, \cdots, 6$, where:

$$\Psi_1(x, y) = \frac{R}{\sqrt{a^2 + x^2 + y^2}}(a, x, y), \tag{4.1}$$

$$\Psi_2(x, y) = \frac{R}{\sqrt{a^2 + x^2 + y^2}}(-x, a, y), \tag{4.2}$$

$$\Psi_3(x, y) = \frac{R}{\sqrt{a^2 + x^2 + y^2}}(-a, -x, y), \tag{4.3}$$

$$\Psi_4(x, y) = \frac{R}{\sqrt{a^2 + x^2 + y^2}}(x, -a, y), \tag{4.4}$$

$$\Psi_5(x, y) = \frac{R}{\sqrt{a^2 + x^2 + y^2}}(-y, x, a), \tag{4.5}$$

$$\Psi_6(x, y) = \frac{R}{\sqrt{a^2 + x^2 + y^2}}(y, x, -a), \tag{4.6}$$

$$D\Psi_1(x, y) = \frac{R}{(a^2 + x^2 + y^2)^{3/2}} \begin{bmatrix} -ax & -ay \\ a^2 + y^2 & -xy \\ -xy & a^2 + x^2 \end{bmatrix} \tag{4.7}$$

$$D\Psi_2(x,y) = \frac{R}{(a^2+x^2+y^2)^{3/2}} \begin{bmatrix} -(a^2+y^2) & xy \\ -ax & -ay \\ -xy & a^2+x^2 \end{bmatrix} \tag{4.8}$$

$$D\Psi_3(x,y) = \frac{R}{(a^2+x^2+y^2)^{3/2}} \begin{bmatrix} ax & ay \\ -(a^2+y^2) & xy \\ -xy & a^2+x^2 \end{bmatrix} \tag{4.9}$$

$$D\Psi_4(x,y) = \frac{R}{(a^2+x^2+y^2)^{3/2}} \begin{bmatrix} a^2+y^2 & -xy \\ ax & ay \\ -xy & a^2+x^2 \end{bmatrix} \tag{4.10}$$

$$D\Psi_5(x,y) = \frac{R}{(a^2+x^2+y^2)^{3/2}} \begin{bmatrix} xy & -(a^2+x^2) \\ a^2+y^2 & -xy \\ -ax & -ay \end{bmatrix} \tag{4.11}$$

$$D\Psi_6(x,y) = \frac{R}{(a^2+x^2+y^2)^{3/2}} \begin{bmatrix} -xy & a^2+x^2 \\ a^2+y^2 & -xy \\ ax & ay \end{bmatrix} \tag{4.12}$$

$$\boldsymbol{g}_1(x,y;p) = D\Psi_p(x,y)\begin{bmatrix}1\\0\end{bmatrix}, \boldsymbol{g}_2(x,y;p) = D\Psi_p(x,y)\begin{bmatrix}0\\1\end{bmatrix}, \tag{4.13}$$

$\{\boldsymbol{g}_1(x,y;p), \boldsymbol{g}_2(x,y;p)\} \subset T_{\Psi_p(x,y)}\mathbb{S}^2_R$, $\forall (x,y) \in [-a,a]\times[-a,a]$

$$[D\Psi_p(x,y)]^T D\Psi_p(x,y) = \frac{R^2}{(a^2+x^2+y^2)^2} \begin{bmatrix} a^2+x^2 & -xy \\ -xy & a^2+y^2 \end{bmatrix} \tag{4.14}$$

Hence, it makes sense to define the matrix $G_\Psi(x,y) = [D\Psi_p(x,y)]^T D\Psi_p(x,y)$ which is known as metric tensor. It is easy to see that:

$$G_\Psi(x,y) = \begin{bmatrix} \langle \boldsymbol{g}_1(x,y;p), \boldsymbol{g}_1(x,y;p)\rangle & \langle \boldsymbol{g}_1(x,y;p), \boldsymbol{g}_2(x,y;p)\rangle \\ \langle \boldsymbol{g}_1(x,y;p), \boldsymbol{g}_2(x,y;p)\rangle & \langle \boldsymbol{g}_2(x,y;p), \boldsymbol{g}_2(x,y;p)\rangle \end{bmatrix} \tag{4.15}$$

and that $G_\Psi(x,y)$ is positive-definite, $\forall (x,y) \in [-a,a]\times[-a,a]$. The Jacobian of the metric tensor $G_\Psi(x,y)$ is then given by:

$$\sqrt{|\det G_\Psi(x,y)|} = \frac{R^2}{(a^2+x^2+y^2)^{3/2}} a \tag{4.16}$$

4.2 Equiangular cubed-sphere

We consider again $a = \frac{R}{\sqrt{3}}$ and we define the family of maps $\Phi_p : [-\frac{\pi}{4}, \frac{\pi}{4}]\times[-\frac{\pi}{4}, \frac{\pi}{4}] \to \mathbb{S}^2_R$, $p = 1, \cdots, 6$, given by $\Phi_p(x, y) = \Psi_p(a \tan x, a \tan y)$. By the chain rule:

$$D\Phi_p(x, y) = a \begin{bmatrix} \frac{1}{\cos^2 x} & 0 \\ 0 & \frac{1}{\cos^2 y} \end{bmatrix} D\Psi_p(a \tan x, a \tan y) \tag{4.17}$$

$$\boldsymbol{r}_1(x, y; p) = D\Phi_p(x, y) \begin{bmatrix} 1 \\ 0 \end{bmatrix} = \frac{a}{\cos^2 x} \boldsymbol{g}_1(\tan x, \tan y; p), \tag{4.18}$$

$$\boldsymbol{r}_2(x, y; p) = D\Phi_p(x, y) \begin{bmatrix} 0 \\ 1 \end{bmatrix} = \frac{a}{\cos^2 y} \boldsymbol{g}_2(\tan x, \tan y; p) \tag{4.19}$$

Hence, it makes sense to define the matrix

$$G_\Phi(x, y) = [D\Phi_p(x, y)]^T D\Phi_p(x, y) \tag{4.20}$$

$$= a^2 [D\Psi_p(a \tan x, a \tan y)]^T \begin{bmatrix} \frac{1}{\cos^4 x} & 0 \\ 0 & \frac{1}{\cos^4 y} \end{bmatrix} D\Psi_p(a \tan x, a \tan y) \tag{4.21}$$

which is known as metric tensor.

$\{\boldsymbol{r}_1(x, y; p), \boldsymbol{r}_{2,p}(x, y; p)\} \subset T_{\Phi_p(x,y)}\mathbb{S}^2_R$, $\forall (x, y) \in [-\frac{\pi}{4}, \frac{\pi}{4}] \times [-\frac{\pi}{4}, \frac{\pi}{4}]$

It is easy to see that:

$$G_\Phi(x, y) = \begin{bmatrix} \langle \boldsymbol{r}_1(x, y; p), \boldsymbol{r}_1(x, y; p) \rangle & \langle \boldsymbol{r}_1(x, y; p), \boldsymbol{r}_2(x, y; p) \rangle \\ \langle \boldsymbol{r}_1(x, y; p), \boldsymbol{r}_2(x, y; p) \rangle & \langle \boldsymbol{r}_2(x, y; p), \boldsymbol{r}_2(x, y; p) \rangle \end{bmatrix} \tag{4.22}$$

and that $G_\Phi(x, y)$ is positive-definite, $\forall (x, y) \in [-\frac{\pi}{4}, \frac{\pi}{4}]\times[-\frac{\pi}{4}, \frac{\pi}{4}]$. The Jacobian of the metric tensor $G_\Phi(x, y)$ is then given by:

$$\sqrt{|\det G_\Phi(x, y)|} = \frac{a}{\cos^2 x \cos^2 y} \frac{R^2}{(a^2 + a^2 \tan^2 x + a^2 \tan^2 y)^{3/2}} a \tag{4.23}$$

$$= \frac{R^2}{\cos^2 x \cos^2 y} \frac{1}{(1 + \tan^2 x + \tan^2 y)^{3/2}} \tag{4.24}$$

Chapter 5

Cubed-sphere finite-volume methods

To be written!

5.1 To be written

Chapter 6

Future work

Since the advection finite volume on the cubed-sphere has been already implemented, we are currently investigating the interpolation/reconstruction of the scalar field at the cube edges aiming to reduce the numerical noises that we observed in some advection test cases.

We also aim to study and implement the shallow-water finite volume model on the sphere introduced by Lin and Rood (1997) and extend it to cubed-sphere following Putman and Lin, 2007. We also shall investigate some modifications on the cubed-sphere such as the equal-edge cubed-sphere proposed by Chen, 2021 and the cubed-sphere with panels overlapping.

Regarding scientific conferences, we intend to attend the PDEs on the sphere 2023 conference (last edition webpage: https://www.dwd.de/EN/specialusers/research_education/seminar/2021/pdes_on_the_sphere/pdes_2020_en_node.html), which will take place in France around July 2023. We aim to present some of the results obtained in this research.

We intend to do a two weeks scientific visit to the researcher Rańcic from NOAA (National Oceanic and Atmospheric Administration), with whom we expect to do a collaborative work on cubed-sphere finite volume schemes.

Appendix A

Finite-difference estimatives

This appendix aims to prove all finite-difference error estimations used throughout this text. All the proves are very simple and consist of applying Taylor's expansions, as it is usual when showing the order of accuracy of many numerical schemes.

Lemma A.1. *Let $F \in C^5([a,b])$, $x_0 \in]a,b[$ and $h > 0$ such that $[x_0 - 2h, x_0 + 2h] \subset [a,b]$. Then, the following identity holds:*

$$F'(x_0) = \frac{4}{3}\left(\frac{F(x_0+h) - F(x_0-h)}{2h}\right) - \frac{1}{3}\left(\frac{F(x_0+2h) - F(x_0-2h)}{4h}\right) + Ch^4, \qquad \text{(A.1)}$$

where C is a constant that depends only on F and h.

Proof. Given $\delta \in]0, 2h]$, then $x_0 + \delta \in]x_0, x_0 + 2h]$ and $x_0 - \delta \in]x_0 - 2h, x_0]$. Then, we get using the Taylor expansion of F:

$$F(x_0+\delta) = F(x_0) + F'(x_0)\delta + F^{(2)}(x_0)\frac{\delta^2}{2} + F^{(3)}(x_0)\frac{\delta^3}{3!} + F^{(4)}(x_0)\frac{\delta^3}{4!} + F^{(5)}(\theta_\delta)\frac{\delta^5}{5!} \quad \theta_\delta \in [x_0, x_0+\delta],$$
$$F(x_0-\delta) = F(x_0) - F'(x_0)\delta + F^{(2)}(x_0)\frac{\delta^2}{2} - F^{(3)}(x_0)\frac{\delta^3}{3!} + F^{(4)}(x_0)\frac{\delta^4}{4!} - F^{(5)}(\theta_{-\delta})\frac{\delta^5}{5!}, \quad \theta_{-\delta} \in [x_0-\delta, x_0].$$

Thus:

$$\frac{F(x_0+\delta) - F(x_0-\delta)}{2\delta} = F'(x_0) + F^{(3)}(x_0)\frac{\delta^2}{3!} + \left(F^{(5)}(\theta_\delta) + F^5(\theta_{-\delta})\right)\frac{\delta^4}{2\cdot 5!}, \qquad \text{(A.2)}$$

Applying Equation (A.2) for $\delta = h$ and $\delta = 2h$, we get, respectively:

$$\frac{F(x_0+h) - F(x_0-h)}{2h} = F'(x_0) + F^{(3)}(x_0)\frac{h^2}{3!} + \left(F^{(5)}(\theta_h) + F^{5)}(\theta_{-h})\right)\frac{h^4}{2\cdot 5!}, \quad \theta_h \in [x_0, x_0+h], \quad \theta_{-h} \in [x_0-h, x_0], \qquad \text{(A.3)}$$

and

$$\frac{F(x_0+2h)-F(x_0-2h)}{4h} = F'(x_0) + F^{(3)}(x_0)\frac{4h^2}{3!} + \left(F^{(5)}(\theta_{2h}) + F^{(5)}(\theta_{-2h})\right)\frac{16h^4}{2\cdot 5!}, \quad \theta_{2h} \in [x_0, x_0+2h], \quad \theta_{-2h} \in [x_0-2h, x_0]. \tag{A.4}$$

Using Equations (A.3) and (A.4), we obtain:

$$\frac{4}{3}\left(\frac{F(x_0+h)-F(x_0-h)}{2h}\right) = \frac{4}{3}F'(x_0) + F^{(3)}(x_0)\frac{4h^2}{3\cdot 3!} + \left(F^{(5)}(\theta_h) + F^{(5)}(\theta_{-h})\right)\frac{h^4}{2\cdot 5!}, \tag{A.5}$$

$$\frac{1}{3}\left(\frac{F(x_0+2h)-F(x_0-2h)}{4h}\right) = \frac{1}{3}F'(x_0) + F^{(3)}(x_0)\frac{4h^2}{3\cdot 3!} + \left(F^{(5)}(\theta_{2h}) + F^{(5)}(\theta_{-2h})\right)\frac{16h^4}{3\cdot 2\cdot 5!} \tag{A.6}$$

Subtracting Equation (A.6) from Equation (A.5) we get the desired Equation (A.1) with

$$C = \frac{1}{240}\left(F^{(5)}(\theta_h) + F^{(5)}(\theta_{-h})\right) - \frac{1}{45}\left(F^{(5)}(\theta_{2h}) + F^{(5)}(\theta_{-2h})\right), \tag{A.7}$$

where $\theta_h \in [x_0, x_0+h], \theta_{-h} \in [x_0-h, x_0]$, $\theta_{2h} \in [x_0, x_0+2h], \theta_{-2h} \in [x_0-2h, x_0]$, which concludes the proof.

Lemma A.2. *Let $F \in C^4([a,b])$, $x_0 \in]a,b[$ and $h > 0$ such that $[x_0-2h, x_0+3h] \subset [a,b]$. Then, the following identity holds:*

$$F''(x_0) = \frac{-2F(x_0-2h) + 15F(x_0-h) - 28F(x_0) + 20F(x_0+h) - 6F(x_0+2h) + F(x_0+3h)}{6h^2} + Ch^2, \tag{A.8}$$

where C is a constant that depends only on F and h.

Proof. From the Taylor's expansion, we have:

$$\begin{aligned}
F(x_0-2h) &= F(x_0) - 2F'(x_0)h + 2F^{(2)}(x_0)h^2 - \frac{8}{6}F^{(3)}(x_0)h^3 + \frac{16}{24}F^{(4)}(\theta_{-2h})h^4,\\
F(x_0-h) &= F(x_0) - F'(x_0)h + \frac{1}{2}F^{(2)}(x_0)h^2 - \frac{1}{6}F^{(3)}(x_0)h^3 + \frac{1}{24}F^{(4)}(\theta_{-h})h^4,\\
F(x_0+h) &= F(x_0) + F'(x_0)h + \frac{1}{2}F^{(2)}(x_0)h^2 + \frac{1}{6}F^{(3)}(x_0)h^3 + \frac{1}{24}F^{(4)}(\theta_h)h^4,\\
F(x_0+2h) &= F(x_0) + 2F'(x_0)h + 2F^{(2)}(x_0)h^2 + \frac{8}{6}F^{(3)}(x_0)h^3 + \frac{16}{24}F^{(4)}(\theta_{2h})h^4,\\
F(x_0+3h) &= F(x_0) + 3F'(x_0)h + \frac{9}{2}F^{(2)}(x_0)h^2 + \frac{27}{6}F^{(3)}(x_0)h^3 + \frac{81}{24}F^{(4)}(\theta_{3h})h^4,
\end{aligned}$$

where $\theta_{-2h} \in [x_0-2h, x_0-h], \theta_{-h} \in [x_0-h, x_0], \theta_h \in [x_0, x_0+h], \theta_{2h} \in [x_0+h, x_0+2h], \theta_{3h} \in [x_0+2h, x_0+3h]$. Multiplying these equations by their respective coefficients given in

Equation (A.8), one get:

$$
\begin{aligned}
-2F(x_0-2h) &= -2F(x_0) + 4F'(x_0)h - 4F^{(2)}(x_0)h^2 + \frac{16}{6}F^{(3)}(x_0)h^3 - \frac{32}{24}F^{(4)}(\theta_{-2h})h^4,\\
15F(x_0-h) &= 15F(x_0) - 15F'(x_0)h + \frac{15}{2}F^{(2)}(x_0)h^2 - \frac{15}{6}F^{(3)}(x_0)h^3 + \frac{15}{24}F^{(4)}(\theta_{-h})h^4,\\
-28F(x_0) &= -28F(x_0),\\
20F(x_0+h) &= 20F(x_0) + 20F'(x_0)h + 10F^{(2)}(x_0)h^2 + \frac{20}{6}F^{(3)}(x_0)h^3 + \frac{20}{24}F^{(4)}(\theta_{h})h^4,\\
-6F(x_0+2h) &= -6F(x_0) - 12F'(x_0)h - 12F^{(2)}(x_0)h^2 - 8F^{(3)}(x_0)h^3 - \frac{96}{24}F^{(4)}(\theta_{2h})h^4,\\
F(x_0+3h) &= F(x_0) + 3F'(x_0)h + \frac{9}{2}F^{(2)}(x_0)h^2 + \frac{27}{6}F^{(3)}(x_0)h^3 + \frac{81}{24}F^{(4)}(\theta_{3h})h^4.
\end{aligned}
$$

Summing all these equations, we get the derised Formula (A.8) with C given by:

$$
C = \frac{1}{24}\left(32F^{(4)}(\theta_{-2h}) - 15F^{(4)}(\theta_{-h}) - 20F^{(4)}(\theta_h) + 96F^{(4)}(\theta_{2h}) - 81F^{(4)}(\theta_{3h})\right), \tag{A.9}
$$

which concludes the proof.

Lemma A.3. *Let $F \in C^4([a,b])$, $x_0 \in]a,b[$ and $h > 0$ such that $[x_0-2h, x_0+3h] \subset [a,b]$. Then, the following identity holds:*

$$
F^{(3)}(x_0) = \frac{F(x_0-2h) - 7F(x_0-h) + 16F(x_0) - 16F(x_0+h) + 7F(x_0+2h) - F(x_0+3h)}{2h^3} + Ch, \tag{A.10}
$$

where C is a constant that depends only on F and h.

Proof. From the Taylor's expansion, we have:

$$
\begin{aligned}
F(x_0-2h) &= F(x_0) - 2F'(x_0)h + 2F^{(2)}(x_0)h^2 - \frac{8}{6}F^{(3)}(x_0)h^3 + \frac{16}{24}F^{(4)}(\theta_{-2h})h^4,\\
F(x_0-h) &= F(x_0) - F'(x_0)h + \frac{1}{2}F^{(2)}(x_0)h^2 - \frac{1}{6}F^{(3)}(x_0)h^3 + \frac{1}{24}F^{(4)}(\theta_{-h})h^4,\\
F(x_0+h) &= F(x_0) + F'(x_0)h + \frac{1}{2}F^{(2)}(x_0)h^2 + \frac{1}{6}F^{(3)}(x_0)h^3 + \frac{1}{24}F^{(4)}(\theta_{h})h^4,\\
F(x_0+2h) &= F(x_0) + 2F'(x_0)h + 2F^{(2)}(x_0)h^2 + \frac{8}{6}F^{(3)}(x_0)h^3 + \frac{16}{24}F^{(4)}(\theta_{2h})h^4,\\
F(x_0+3h) &= F(x_0) + 3F'(x_0)h + \frac{9}{2}F^{(2)}(x_0)h^2 + \frac{27}{6}F^{(3)}(x_0)h^3 + \frac{81}{24}F^{(4)}(\theta_{3h})h^4,
\end{aligned}
$$

where $\theta_{-2h} \in [x_0-2h, x_0-h]$, $\theta_{-h} \in [x_0-h, x_0]$, $\theta_h \in [x_0, x_0+h]$, $\theta_{2h} \in [x_0+h, x_0+2h]$, $\theta_{3h} \in [x_0+2h, x_0+3h]$. Multiplying these equations by their respective coefficients given in Equation (A.10), one get:

$$
\begin{aligned}
F(x_0-2h) &= F(x_0) - 2F'(x_0)h + \frac{4}{2}F^{(2)}(x_0)h^2 - \frac{8}{6}F^{(3)}(x_0)h^3 + \frac{16}{24}F^{(4)}(\theta_{-2h})h^4,\\
-7F(x_0-h) &= -7F(x_0) + 7F'(x_0)h - \frac{7}{2}F^{(2)}(x_0)h^2 + \frac{7}{6}F^{(3)}(x_0)h^3 - \frac{7}{24}F^{(4)}(\theta_{-h})h^4,\\
16F(x_0) &= 16F(x_0),\\
-16F(x_0+h) &= -16F(x_0) - 16F'(x_0)h - \frac{16}{2}F^{(2)}(x_0)h^2 - \frac{16}{6}F^{(3)}(x_0)h^3 - \frac{16}{24}F^{(4)}(\theta_h)h^4,\\
7F(x_0+2h) &= 7F(x_0) + 14F'(x_0)h + \frac{28}{2}F^{(2)}(x_0)h^2 + \frac{56}{6}F^{(3)}(x_0)h^3 + \frac{112}{24}F^{(4)}(\theta_{2h})h^4,\\
-F(x_0+3h) &= -F(x_0) - 3F'(x_0)h - \frac{9}{2}F^{(2)}(x_0)h^2 - \frac{27}{6}F^{(3)}(x_0)h^3 - \frac{81}{24}F^{(4)}(\theta_{3h})h^4.
\end{aligned}
$$

Summing all these equations, we have:

$$F(x_0-2h) - 7F(x_0-h) + 16F(x_0) - 16F(x_0+h) + 7F(x_0+2h) - F(x_0+3h) = 2F^{(3)}(x_0)h^3 - 2Ch^4,$$

we get the derised Formula (A.10) with C given by:

$$C = \frac{1}{48}\left(-16F^{(4)}(\theta_{-2h}) + 7F^{(4)}(\theta_{-h}) + 16F^{(4)}(\theta_h) - 112F^{(4)}(\theta_{2h}) + 81F^{(4)}(\theta_{3h})\right), \quad \text{(A.11)}$$

which concludes the proof.

Appendix B

Spherical coordinates and geometry

Given $R > 0$, we denote the sphere of radius R centered at the origin of $\mathbb{R}^3$:

$$\mathbb{S}^2_R = \{(X, Y, Z) \in \mathbb{R}^3 \ : \ X^2 + Y^2 + Z^2 = R^2\}.$$

The tangent space at $P \in \mathbb{S}^2_R$ by $T_P\mathbb{S}^2$. It is easy to see that:

$$T_P\mathbb{S}^2_R = \{Q \in \mathbb{R}^3 \ : \ \langle P, Q\rangle = 0\},$$

where $\langle \cdot, \cdot \rangle$ denotes the standard inner product of $\mathbb{R}^3$. The tangent bundle is denoted by:

$$T\mathbb{S}^2_R = \bigcup_{P \in \mathbb{S}^R_2} T_P\mathbb{S}^2_R.$$

We are going to consider three ways to represent an element of $\mathbb{S}^2_R$: using (X, Y, Z) coordinates, or using (λ, ϕ) latitude-longitude coordinates, or, at last, using the cubed-sphere coordinates (x, y, p), where (x, y) are the cube face coordinates and $p \in \{1, 2, \cdots, 6\}$ stands for a cube panel, as presented in Chapter 4.

B.1 Tangent vectors

Let us consider $P \in \mathbb{S}^2_R$, we consider the projection on the tangent space $T_P\mathbb{S}^2_R$ which is given by:

$$\Pi_P(Q) = \frac{\langle P, Q\rangle}{R} P - Q$$

We introduce the tangent vectors at $\Psi_p(x, y)$ given by: $\boldsymbol{g}_x(x, y; p) = \Pi_P(\Psi_p(x + \Delta x, y))$, $\boldsymbol{g}_y(x, y; p) = \Pi_P(\Psi_p(x, y+\Delta y))$, where $P = \Psi_p(x, y+\Delta y)$. We then introduce the normalized vectors:

$$\boldsymbol{e}_x(x, y; p) = \frac{\boldsymbol{g}_x(x, y; p)}{\|\boldsymbol{g}_x(x, y; p)\|}, \quad \boldsymbol{e}_y(x, y; p) = \frac{\boldsymbol{g}_y(x, y; p)}{\|\boldsymbol{g}_y(x, y; p)\|},$$

where $\|\cdot\|$ is the Euclidean norm. It can be shown that the tangent vector of the geodesic from $\Psi_p(x,y)$ from $\Psi_p(x+\Delta x,y)$ is a multiple of $\boldsymbol{e}_x$ and the tangent vector of the geodesic from $\Psi_p(x,y)$ from $\Psi_p(x,y+\Delta y)$ is a multiple of $\boldsymbol{e}_y$. Thus, this process using the projection operator on the tangent space allow us to compute the unit tangent vectors for any cubed-sphere mapping gridlines at a given point.

B.2 Conversions between latitude-longitude and contravariant coordinates

We consider the latitude-longitude mapping $\Psi_{ll} : [0,2\pi]\times[-\frac{\pi}{2},\frac{\pi}{2}] \to \mathbb{S}^2_R$, given by:

$$X(\lambda,\phi) = R\cos\phi\cos\lambda, \tag{B.1}$$
$$Y(\lambda,\phi) = R\cos\phi\sin\lambda, \tag{B.2}$$
$$Z(\lambda,\phi) = R\sin\phi, \tag{B.3}$$

The derivative or Jacobian matrix of the mapping Ψ_{ll} is given by:

$$D\Psi_{ll}(\lambda,\phi) = R\begin{bmatrix} -\cos\phi\sin\lambda & -\sin\phi\cos\lambda \\ \cos\phi\cos\lambda & \sin\phi\sin\lambda \\ 0 & \cos\phi \end{bmatrix} \tag{B.4}$$

Using this matrix columns, we can define the tangent vectors:

$$\boldsymbol{g}_\lambda(\lambda,\phi) = D\Psi_{ll}(\lambda,\phi)\begin{bmatrix}1\\0\end{bmatrix}, \quad \boldsymbol{g}_\phi(\lambda,\phi) = D\Psi_{ll}(\lambda,\phi)\begin{bmatrix}0\\1\end{bmatrix}, \tag{B.5}$$

We normalize the vectors $\boldsymbol{g}_\lambda$ and $\boldsymbol{g}_\phi$ and we obtain unit tangent vectors on the sphere at $\Phi_{ll}(\lambda,\phi)$:

$$\boldsymbol{e}_\lambda(\lambda,\phi) = \begin{bmatrix}-\sin\lambda\\ \cos\lambda\\ 0\end{bmatrix}, \quad \boldsymbol{e}_\phi(\lambda,\phi) = \begin{bmatrix}-\sin\phi\cos\lambda\\ -\sin\phi\sin\lambda\\ \cos\phi\end{bmatrix}, \tag{B.6}$$

Let us consider a tangent vector field $\boldsymbol{u} : \mathbb{S}^2_R \to T\mathbb{S}^2_R$ on the sphere, *i.e.*, $\boldsymbol{u}(P)\in T_P\mathbb{S}^2_R$, $\forall P\in\mathbb{S}^2_R$. We may express this vector fields in latitude-longitude coordinates as:

$$\boldsymbol{u}(\lambda,\phi) = u_\lambda(\lambda,\phi)\boldsymbol{e}_\lambda(\lambda,\phi) + v_\phi(\lambda,\phi)\boldsymbol{e}_\phi(\lambda,\phi). \tag{B.7}$$

Or, we may also represent this vector field using the basis obtained by cubed-sphere coordinates:

$$\boldsymbol{u}(x,y;p) = \tilde{u}(x,y;p)\boldsymbol{e}_x(x,y;p) + \tilde{v}(x,y;p)\boldsymbol{e}_y(x,y;p). \tag{B.8}$$

This representation is known as contravariant representation. In order to relate the latitude-

longitude representation with the contravariant representation, we notice that:

$$\boldsymbol{e_x}(x,y;p) = \langle \boldsymbol{e}_x, \boldsymbol{e}_\lambda \rangle \boldsymbol{e}_\lambda(\lambda,\phi) + \langle \boldsymbol{e}_x, \boldsymbol{e}_\phi \rangle \boldsymbol{e}_\phi(\lambda,\phi), \tag{B.9}$$

$$\boldsymbol{e_y}(x,y;p) = \langle \boldsymbol{e}_y, \boldsymbol{e}_\lambda \rangle \boldsymbol{e}_\lambda(\lambda,\phi) + \langle \boldsymbol{e}_y, \boldsymbol{e}_\phi \rangle \boldsymbol{e}_\phi(\lambda,\phi), \tag{B.10}$$

which holds since the vectors $\boldsymbol{e}_\lambda(\lambda,\phi)$ and $\boldsymbol{e}_\phi(\lambda,\phi)$ are orthogonal. Replacing Equations (B.9) and (B.10) in Equation (B.8), we obtain the values (u_λ, v_ϕ) in terms of the contravariant components $(\tilde{u},\tilde{v})$ as the following matrix equation:

$$\begin{bmatrix} u_\lambda(\lambda,\phi) \\ v_\phi(\lambda,\phi) \end{bmatrix} = \begin{bmatrix} \langle \boldsymbol{e}_x, \boldsymbol{e}_\lambda \rangle & \langle \boldsymbol{e}_y, \boldsymbol{e}_\lambda \rangle \\ \langle \boldsymbol{e}_x, \boldsymbol{e}_\phi \rangle & \langle \boldsymbol{e}_y, \boldsymbol{e}_\phi \rangle \end{bmatrix} \begin{bmatrix} \tilde{u}(x,y;p) \\ \tilde{v}(x,y;p) \end{bmatrix}. \tag{B.11}$$

Conversely, we may express the contravariant components in terms of latitude-longitude components by inverting Equation (B.11):

$$\begin{bmatrix} \tilde{u}(x,y;p) \\ \tilde{v}(x,y;p) \end{bmatrix} = \frac{1}{\langle \boldsymbol{e}_x, \boldsymbol{e}_\lambda \rangle \langle \boldsymbol{e}_y, \boldsymbol{e}_\phi \rangle - \langle \boldsymbol{e}_y, \boldsymbol{e}_\lambda \rangle \langle \boldsymbol{e}_x, \boldsymbol{e}_\phi \rangle} \begin{bmatrix} \langle \boldsymbol{e}_y, \boldsymbol{e}_\phi \rangle & -\langle \boldsymbol{e}_y, \boldsymbol{e}_\lambda \rangle \\ -\langle \boldsymbol{e}_x, \boldsymbol{e}_\phi \rangle & \langle \boldsymbol{e}_x, \boldsymbol{e}_\lambda \rangle \end{bmatrix} \begin{bmatrix} u_\lambda(\lambda,\phi) \\ v_\phi(\lambda,\phi) \end{bmatrix}. \tag{B.12}$$

B.3 Covariant/contravariant conversion

Given Equation Let us consider again a tangent vector field $\boldsymbol{u} : \mathbb{S}^2_R \to T\mathbb{S}^2_R$ on the sphere, the contravariant representation of $\boldsymbol{u}$ is given by Equation (B.8). The covariant components (u,v) are given by:

$$u(x,y;p) = \langle \boldsymbol{u}(x,y;p), e_x(x,y;p) \rangle, \tag{B.13}$$

$$v(x,y;p) = \langle \boldsymbol{u}(x,y;p), e_y(x,y;p) \rangle. \tag{B.14}$$

Replacing Equation (B.8) in Equations (B.13) and (B.14) we obtain the relation covariant components in terms of the contravariant terms:

$$\begin{bmatrix} u(x,y;p) \\ v(x,y;p) \end{bmatrix} = \begin{bmatrix} 1 & \langle \boldsymbol{e}_x, \boldsymbol{e}_y \rangle \\ \langle \boldsymbol{e}_x, \boldsymbol{e}_y \rangle & 1 \end{bmatrix} \begin{bmatrix} \tilde{u}(x,y;p) \\ \tilde{v}(x,y;p) \end{bmatrix}. \tag{B.15}$$

Denoting the angle between $\boldsymbol{e}_x$ and $\boldsymbol{e}_y$ by α, we have $\langle \boldsymbol{e}_x, \boldsymbol{e}_y \rangle = \cos\alpha$. Thus, we may express the contravariant components in terms of the covariant terms inverting Equation (B.15):

$$\begin{bmatrix} \tilde{u}(x,y;p) \\ \tilde{v}(x,y;p) \end{bmatrix} = \frac{1}{\sin^2\alpha} \begin{bmatrix} 1 & -\cos\alpha \\ -\cos\alpha & 1 \end{bmatrix} \begin{bmatrix} u(x,y;p) \\ v(x,y;p) \end{bmatrix}. \tag{B.16}$$

Notice that combining Equations (B.15) and (B.16) with Equations (B.11) and (B.12) one may get relations between the latitude-longitude components and the covariant components.

Appendix C

Code avaibility

The codes needed for this work have been built openly at GitHub. The PPM implementation for the one-dimensional advection equation is available at https://github.com/luanfs/py-ppm. The dimension-splitting implementation for the advection equation on the plane is available at https://github.com/luanfs/py-dimension-splitting. At last, all the grid tools for the cubed sphere, including the finite volume model on this grid, is available at https://github.com/luanfs/py-cubed-sphere.

The implementation of the high-order schemes for the moist shallow-water model on Voronoi grids may be accessed at https://github.com/pedrospeixoto/iModel.

Finally, the report for the qualification exam has also been built at GitHub in the following repository: https://github.com/luanfs/doc-qualification.

All the contents in GithHub's repositories shown previously are under constant development.

References

Arakawa, A., & Lamb, V. R. (1977). Computational design of the basic dynamical processes of the ucla general circulation model. In *General circulation models of the atmosphere* (pp. 173–265). Elsevier. https://doi.org/https://doi.org/10.1016/B978-0-12-460817-7.50009-4. (Cit. on p. 4)

Barros, S., Dent, D., Isaksen, L., Robinson, G., Mozdzynski, G., & Wollenweber, F. (1995). The ifs model: A parallel production weather code. *Parallel Computing*, *21*(10), 1621–1638. https://doi.org/https://doi.org/10.1016/0167-8191(96)80002-0 (cit. on p. 3)

Benacchio, T., & Wood, N. (2016). Semi-implicit semi-lagrangian modelling of the atmosphere: A met office perspective. *Communications in Applied and Industrial Mathematics*, *7*(3), 4–25. https://doi.org/doi:10.1515/caim-2016-0020 (cit. on p. 1)

Carpenter, R. L., Droegemeier, K. K., Woodward, P. R., & Hane, C. E. (1990). Application of the piecewise parabolic method (ppm) to meteorological modeling. *Monthly Weather Review*, *118*(3), 586–612. https://doi.org/10.1175/1520-0493(1990)118<0586:AOTPPM>2.0.CO;2 (cit. on pp. 4, 12)

Chen, X. (2021). The lmars based shallow-water dynamical core on generic gnomonic cubed-sphere geometry [e2020MS002280 2020MS002280]. *Journal of Advances in Modeling Earth Systems*, *13*(1), e2020MS002280. https://doi.org/https://doi.org/10.1029/2020MS002280 (cit. on p. 35)

Colella, P., & Woodward, P. R. (1984). The piecewise parabolic method (ppm) for gas-dynamical simulations. *Journal of Computational Physics*, *54*(1), 174–201. https://doi.org/https://doi.org/10.1016/0021-9991(84)90143-8 (cit. on pp. 4, 12, 14, 19)

Cooley, J. W., & Tukey, J. W. (1965). An algorithm for the machine calculation of complex fourier series. *Mathematics of Computation*, *19*(90), 297–301. http://www.jstor.org/stable/2003354 (cit. on p. 2)

Dennis, J., Edwards, J., Evans, K., Guba, O., Lauritzen, P., Mirin, A., St-Cyr, A., Taylor, M., & Worley, P. (2012). Cam-se: A scalable spectral element dynamical core for the community atmosphere model. *Internat. J. High Perf. Comput. Appl.*, *26*, 74–89. https://doi.org/10.1177/1094342011428142 (cit. on p. 4)

Eliasen, E., Machenhauer, B., & Rasmussen, E. (1970). On a numerical method for integration of the hydrodynamical equations wirh a spectral representation of the horizontal fields. https://doi.org/10.13140/RG.2.2.13894.88645 (cit. on p. 2)

Figueroa, S., Bonatti, J., Kubota, P., Grell, G., Morrison, H., R. M. Barros, S., Fernandez, J., Ramirez-Gutierrez, E., Siqueira, L., Luzia, G., Silva, J., Silva, J., Pendharkar, J., Capistrano, V., Alvim, D., Enore, D., Diniz, F., Satyamurty, P., Cavalcanti, I., & Panetta, J. (2016). The brazilian global atmospheric model (bam): Performance for tropical rainfall forecasting and sensitivity to convective scheme and horizontal resolution. *Weather Forecast.*, *31(5)*, 1547–1572. https://doi.org/10.1175/WAF-D-16-0062.1 (cit. on p. 3)

Giraldo, F. X., Kelly, J. F., & Constantinescu, E. M. (2013). Implicit-explicit formulations of a three-dimensional nonhydrostatic unified model of the atmosphere (numa). *SIAM Journal on Scientific Computing*, *35*(5), B1162–B1194. https://doi.org/10.1137/120876034 (cit. on p. 4)

Harris, L. M., & Lin, S.-J. (2013). A two-way nested global-regional dynamical core on the cubed-sphere grid. *Monthly Weather Review*, *141*(1), 283–306. https://doi.org/10.1175/MWR-D-11-00201.1 (cit. on p. 4)

Kent, J., Melvin, T., & Wimmer, G. A. (2022). A mixed finite element discretisation of the shallow water equations. *Geoscientific Model Development Discussions*, *2022*, 1–17. https://doi.org/10.5194/gmd-2022-225 (cit. on p. 4)

Krishnamurti, T., Hardiker, V., Bedi, H., & Ramaswamy, L. (2006). *An introduction to global spectral modeling* (Vol. 35). https://doi.org/10.1007/0-387-32962-5. (Cit. on p. 2)

Lauritzen, P. H., Ullrich, P. A., & Nair, R. D. (2011). In *An introduction to global spectral modeling* (pp. 185–250). Springer New York, NY. https://doi.org/https://doi.org/10.1007/0-387-32962-5. (Cit. on p. 29)

LeVeque, R. J. (1990). *Numerical methods for conservation laws*. Birkhäuser Basel. https://doi.org/10.1007/978-3-0348-5116-9. (Cit. on pp. 7–9, 24)

LeVeque, R. J. (2002). *Finite volume methods for hyperbolic problems*. Cambridge University Press. https://doi.org/10.1017/CBO9780511791253. (Cit. on pp. 7, 11)

Lin, S.-J. (2004). A "vertically lagrangian" finite-volume dynamical core for global models. *Monthly Weather Review*, *132*(10), 2293–2307. https://doi.org/10.1175/1520-0493(2004)132<2293:AVLFDC>2.0.CO;2 (cit. on pp. 4, 27)

Lin, S.-J., Chao, W. C., Sud, Y. C., & Walker, G. K. (1994). A class of the van leer-type transport schemes and its application to the moisture transport in a general circulation model. *Monthly Weather Review*, *122*(7), 1575–1593. https://doi.org/10.1175/1520-0493(1994)122<1575:ACOTVL>2.0.CO;2 (cit. on p. 4)

Lin, S.-J., & Rood, R. B. (1996). Multidimensional flux-form semi-lagrangian transport schemes. *Monthly Weather Review*, *124*(9), 2046–2070. https://doi.org/10.1175/1520-0493(1996)124<2046:MFFSLT>2.0.CO;2 (cit. on pp. 4, 12)

Lin, S.-J., & Rood, R. B. (1997). An explicit flux-form semi-lagrangian shallow-water model on the sphere. *Quarterly Journal of the Royal Meteorological Society*, *123*(544), 2477–2498. https://doi.org/https://doi.org/10.1002/qj.49712354416 (cit. on pp. 4, 27, 35)

Müller, A., Deconinck, W., Kühnlein, C., Mengaldo, G., Lange, M., Wedi, N., Bauer, P., Smolarkiewicz, P. K., Diamantakis, M., Lock, S.-J., Hamrud, M., Saarinen, S., Mozdzynski, G., Thiemert, D., Glinton, M., Bénard, P., Voitus, F., Colavolpe, C., Marguinaud, P., … New, N. (2019). The escape project: Energy-efficient scalable algorithms for weather prediction at exascale. *Geoscientific Model Development*, *12*(10), 4425–4441. https://doi.org/10.5194/gmd-12-4425-2019 (cit. on p. 3)

Nair, R. D., Levy, M. N., & Lauritzen, P. H. (2011). Emerging numerical methods for atmospheric modeling. In *Numerical techniques for global atmospheric models* (pp. 251–311). Springer Berlin Heidelberg. https://doi.org/10.1007/978-3-642-11640-7_9. (Cit. on p. 9)

Nair, R. D., Thomas, S. J., & Loft, R. D. (2005). A discontinuous galerkin transport scheme on the cubed sphere. *Monthly Weather Review*, *133*(4), 814–828. https://doi.org/10.1175/MWR2890.1 (cit. on p. 29)

Orszag, S. A. (1970). Transform method for the calculation of vector-coupled sums: Application to the spectral form of the vorticity equation. *Journal of Atmospheric Sciences*, *27*(6), 890–895. https://doi.org/10.1175/1520-0469(1970)027<0890:TMFTCO>2.0.CO;2 (cit. on p. 2)

Peixoto, P. (2016). Accuracy analysis of mimetic finite volume operators on geodesic grids and a consistent alternative. *J. Comput. Phys.*, *310*, 127–160. https://doi.org/10.1016/j.jcp.2015.12.058 (cit. on p. 5)

Peixoto, P., & Barros, S. R. M. (2013). Analysis of grid imprinting on geodesic spherical icosahedral grids. *J. Comput. Phys.*, *237*, 61–78. https://doi.org/10.1016/j.jcp.2012.11.041 (cit. on p. 5)

Putman, W. M. (2007). *Development of the finite-volume dynamical core on the cubed-sphere* (Doctoral dissertation). Florida State University. Florida, US. http://purl.flvc.org/fsu/fd/FSU_migr_etd-0511. (Cit. on pp. 4, 27)

Putman, W. M., & Lin, S.-J. (2007). Finite-volume transport on various cubed-sphere grids. *Journal of Computational Physics*, *227*(1), 55–78. https://doi.org/https://doi.org/10.1016/j.jcp.2007.07.022 (cit. on pp. 4, 5, 27, 35)

Rančić, M., Purser, R. J., & Mesinger, F. (1996). A global shallow-water model using an expanded spherical cube: Gnomonic versus conformal coordinates. *Quarterly Journal of the Royal Meteorological Society*, *122*(532), 959–982. https://doi.org/https://doi.org/10.1002/qj.49712253209 (cit. on p. 29)

Rančić, M., Purser, R. J., Jović, D., Vasic, R., & Black, T. (2017). A nonhydrostatic multiscale model on the uniform jacobian cubed sphere. *Monthly Weather Review*, *145*(3), 1083–1105. https://doi.org/10.1175/MWR-D-16-0178.1 (cit. on p. 4)

Randall, D. A., Bitz, C. M., Danabasoglu, G., Denning, A. S., Gent, P. R., Gettelman, A., Griffies, S. M., Lynch, P., Morrison, H., Pincus, R., & Thuburn, J. (2018). 100 years of earth system model development. *Meteorological Monographs*, *59*, 12.1–12.66. https://doi.org/10.1175/AMSMONOGRAPHS-D-18-0018.1 (cit. on pp. 1, 3)

Ringler, T., Thuburn, J., Klemp, J., & Skamarock, W. (2010). A unified approach to energy conservation and potential vorticity dynamics on arbitrarily structured C-grids. *J. Comput. Phys.*, *229*, 3065–3090. https://doi.org/10.1016/j.jcp.2009.12.007 (cit. on p. 5)

Ronchi, C., Iacono, R., & Paolucci, P. (1996). The "cubed sphere": A new method for the solution of partial differential equations in spherical geometry. *Journal of Computational Physics*, *124*(1), 93–114. https://doi.org/https://doi.org/10.1006/jcph.1996.0047 (cit. on pp. 4, 29)

Sadourny, R. (1972). Conservative finite-difference approximations of the primitive equations on quasi-uniform spherical grids. *Monthly Weather Review*, *100*(2), 136–144. https://doi.org/10.1175/1520-0493(1972)100<0136:CFAOTP>2.3.CO;2 (cit. on pp. 4, 29)

Samenow, J. (2019). *National weather service launches upgraded, improved global forecast model*. Retrieved July 29, 2022, from https://www.washingtonpost.com/weather/2019/06/12/national-weather-service-launches-upgraded-improved-global-forecast-model/. (Cit. on p. 4)

Santos, L. F., & Peixoto, P. S. (2021). Topography-based local spherical voronoi grid refinement on classical and moist shallow-water finite-volume models. *Geoscientific Model Development*, *14*(11), 6919–6944. https://doi.org/10.5194/gmd-14-6919-2021 (cit. on p. 5)

Skamarock, W., Klemp, J., Duda, M., Fowler, L., Park, S.-H., & Ringler, T. (2012). A multiscale nonhydrostatic atmospheric model using centroidal Voronoi tesselations and C-grid staggering. *Mon. Weather. Rev.*, *140(09)*, 3090–3105. https://doi.org/10.1175/MWR-D-11-00215.1 (cit. on p. 5)

Staniforth, A., & Thuburn, J. (2012). Horizontal grids for global weather and climate prediction models: A review. *Q. J. Roy. Meteor. Soc.*, *138*, 1–26. https://doi.org/10.1002/qj.958 (cit. on p. 3)

Taylor, M., Tribbia, J., & Iskandarani, M. (1997). The spectral element method for the shallow water equations on the sphere. *Journal of Computational Physics*, *130*(1), 92–108. https://doi.org/https://doi.org/10.1006/jcph.1996.5554 (cit. on p. 29)

Thuburn, J. (2011). Conservation in dynamical cores: What, how and why? In *Numerical techniques for global atmospheric models* (pp. 345–355). Springer Berlin Heidelberg. https://doi.org/10.1007/978-3-642-11640-7_11. (Cit. on p. 3)

Thuburn, J., Ringler, T., Skamarock, W., & Klemp, J. (2009). Numerical representation of geostrophic modes on arbitrarily structured C-grids. *J. Comput. Phys.*, *228*, 8321–8335. https://doi.org/10.1016/j.jcp.2009.08.006 (cit. on p. 5)

Ullrich, P. A., Jablonowski, C., Kent, J., Lauritzen, P. H., Nair, R., Reed, K. A., Zarzycki, C. M., Hall, D. M., Dazlich, D., Heikes, R., Konor, C., Randall, D., Dubos, T., Meurdesoif, Y., Chen, X., Harris, L., Kühnlein, C., Lee, V., Qaddouri, A., … Viner, K. (2017). Dcmip2016: A review of non-hydrostatic dynamical core design and intercomparison of participating models. *Geoscientific Model Development*, *10*(12), 4477–4509. https://doi.org/10.5194/gmd-10-4477-2017 (cit. on p. 3)

Van Leer, B. (1977). Towards the ultimate conservative difference scheme. iv. a new approach to numerical convection. *Journal of Computational Physics*, *23*(3), 276–299. https://doi.org/https://doi.org/10.1016/0021-9991(77)90095-X (cit. on pp. 4, 12)

Weller, H. (2012). Controlling the computational modes of the arbitrarily structured c grid, *Mon. Weather. Rev.*, *140(10)*, 3220–3234. https://doi.org/doi.org/10.1175/MWR-D-11-00221.1 (cit. on p. 5)

Whitaker, J. (2015). *Hiwpp non-hydrostatic dynamical core tests: Results from idealized test cases*. Retrieved November 5, 2022, from https://www.weather.gov/media/sti/nggps/HIWPP_idealized_tests-v8%20revised%2005212015.pdf/. (Cit. on p. 4)

Williamson, D. L. (2007). The evolution of dynamical cores for global atmospheric models. *Journal of the Meteorological Society of Japan. Ser. II*, *85B*, 241–269. https://doi.org/10.2151/jmsj.85B.241 (cit. on pp. 1, 2)

Wood, N., Staniforth, A., White, A., Allen, T., Diamantakis, M., Gross, M., Melvin, T., Smith, C., Vosper, S., Zerroukat, M., & Thuburn, J. (2014). An inherently mass-conserving semi-implicit semi-lagrangian discretization of the deep-atmosphere global non-hydrostatic equations. *Quarterly Journal of the Royal Meteorological Society*, *140*(682), 1505–1520. https://doi.org/https://doi.org/10.1002/qj.2235 (cit. on p. 1)

Zheng, Y., & Marguinaud, P. (2018). Simulation of the performance and scalability of message passing interface (mpi) communications of atmospheric models running on exascale supercomputers. *Geoscientific Model Development*, *11*(8), 3409–3426. https://doi.org/10.5194/gmd-11-3409-2018 (cit. on p. 3)